HHS Public Access

Author manuscript

Dev Biol. Author manuscript; available in PMC 2020 June 01.

Published in final edited form as:

Dev Biol. 2019 June 01; 450(1): 47–62. doi:10.1016/j.ydbio.2019.03.011.

Derepression of sonic hedgehog signaling upon *Gpr161* deletion unravels forebrain and ventricular abnormalities

Issei S. Shimada[1,5,*], **Bandarigoda N. Somatilaka**[1], **Sun-Hee Hwang**[1], **Ashley G. Anderson**[2], **John M. Shelton**[3], **Veena Rajaram**[4], **Genevieve Konopka**[2], and **Saikat Mukhopadhyay**[1,*,#]

[1]Department of Cell Biology, University of Texas Southwestern Medical Center, Dallas, Texas, USA 75390.

[2]Department of Neuroscience, University of Texas Southwestern Medical Center, Dallas, Texas, USA 75390.

[3]Department of Internal Medicine, University of Texas Southwestern Medical Center, Dallas, Texas, USA 75390.

[4]Department of Pathology and Laboratory Medicine, Children's Health, University of Texas Southwestern Medical Center, Dallas, Texas, USA 75390.

[5]Present address: Department of Cell Biology, Graduate School of Medical Sciences, Nagoya City University, Nagoya, Japan, 467-8601.

Abstract

Inverse gradients of transcriptional repressors antagonize the transcriptional effector response to morphogens. However, the role of such inverse regulation might not manifest solely from lack of repressors. Sonic hedgehog (Shh) patterns the forebrain by being expressed ventrally; however, absence of antagonizing Gli3 repressor paradoxically cause insufficient pathway activation. Interestingly, lack of the primary cilia-localized G-protein-coupled receptor, Gpr161 increases Shh signaling in the mouse neural tube from coordinated lack of Gli3 repressor and Smoothened-independent activation. Here, by deleting *Gpr161* in mouse neuroepithelial cells and radial glia at early mid-gestation we detected derepression of Shh signaling throughout forebrain, allowing determination of the pathophysiological consequences. Accumulation of cerebrospinal fluid (hydrocephalus) was apparent by birth, although usual causative defects in multiciliated ependymal cells or aqueduct were not seen. Rather, the ventricular surface was expanded (ventriculomegaly) during embryogenesis from radial glial overproliferation. Cortical phenotypes included polymicrogyria in the medial cingulate cortex, increased proliferation of intermediate progenitors and basal radial glia, and altered neocortical cytoarchitectonic structure with increased upper layer and decreased deep layer neurons. Finally, periventricular nodular heterotopia resulted from disrupted neuronal migration, while the radial glial scaffold was unaffected. Overall,

[*]Correspondence: ishimada@med.nagoya-cu.ac.jp (I. S. S.), Saikat.Mukhopadhyay@utsouthwestern.edu (S. M.).
[#]Lead Contact.

suppression of Shh pathway during early mid-gestation prevents ventricular overgrowth, and regulates cortical gyration and neocortical/periventricular cytoarchitecture.

Graphical Abstract

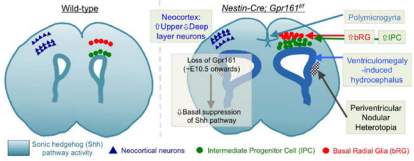

Keywords

Primary cilia; Sonic hedgehog; Gpr161; hydrocephalus; periventricular heterotopia; polymicrogyria

Introduction

Morphogens are secreted signaling molecules that pattern tissues by providing information in time and space (Wolpert, 1969). Morphogens are often inhibited by secreted antagonists (De Robertis, 2006). Alternatively, inverse gradients of transcriptional repressors inhibit transcriptional effector-mediated morphogen responses (Ashe and Briscoe, 2006). The functional consequences of impairing such inverse repressive regulation might not be manifested solely from lack of the repressors. Rather, reciprocal deregulation of both repressor and activator gradients is required for adequately uncovering derepression phenotypes and in understanding the basis of such cross-regulation in morphogenetic pathways.

The Sonic hedgehog (Shh) pathway is organized in a way that the final transcriptional output is determined by post-translational modification of Gli transcription factors into activators or repressors in the presence or absence of Shh, respectively (Goetz and Anderson, 2010). The primary cilia serve as cellular antennae in coordinating extracellular signals with intracellular signaling pathways. Both the Shh-dependent activation and Shh-independent repression pathways are primary cilia-dependent (Goetz and Anderson, 2010; Mukhopadhyay and Rohatgi, 2014). Shh binding to Patched1 (Ptch1), the Shh receptor, results in removal of Ptch1 from cilia, and ciliary enrichment of Smoothened (Smo), enabling pathway activation by formation of Gli2 transcriptional activator. In the absence of Shh, the pathway is basally repressed by formation of Gli3 transcriptional repressor in a protein kinase A (PKA)-dependent manner. The primary cilia-localized orphan G-protein-coupled receptor (GPCR), Gpr161 represses Shh pathway in the neural tube (Mukhopadhyay et al., 2013). Gpr161 increases cAMP in a $G\alpha_S$-coupled manner leading to Gli3 repressor formation (Mukhopadhyay et al., 2013). Gpr161 also anchors the PKA regulatory subunit I α/β (PKA-RI) by its C-terminal tail serving as its own A-kinase anchoring protein (Bachmann et al., 2016). Lack of Gpr161 causes increased Shh signaling from coordinated lack of repressor and Smo-independent activation of the pathway (Mukhopadhyay et al., 2013).

Shh is a key morphogen that patterns the forebrain. Shh is primarily expressed in the basal plate of mid telencephalon extending dorsally into a wedge in the zona limitans intrathalamica and later beneath the medial ganglionic eminences (MGEs) (Shimamura et al., 1995). However, the role of inverse repressive regulation of Shh signaling is unknown during forebrain development. First, lack of the downstream repressor *Gli3* paradoxically does not cause pathway derepression in forebrain (Wang et al., 2014; Yu et al., 2009). Whereas *Gli1* expression is reduced in *Gli3* knockouts (Yu et al., 2009), *NestinCre; Gli3*$^{f/Xt}$ mice exhibit intermediate Shh responsiveness and decreased maximal pathway activity (Wang et al., 2014). Second, *Gli2/3* single or double knockouts are perinatal lethal or lethal by E13.5 (Bai and Joyner, 2001; Blaess et al., 2006; Yu et al., 2009), respectively, preventing dissection of mature phenotypes (Yu et al., 2009). Third, current models using ectopic Shh signaling (Himmelstein et al., 2010; Huang et al., 2007; Komada et al., 2008; Shikata et al., 2011) or overexpression of a constitutively active *SmoM2* mutant (Wang et al., 2016) might not reflect the physiological role of repressive regulation of Shh signaling in telencephalon. Fourth, conditional knockouts of PKA catalytic subunits are technically challenging, as multiple isoforms of α and β need to be deleted conditionally. Finally, conditional lack of Suppressor of fused (Sufu), another negative regulator that restrains Gli3 in the cytoplasm and promotes repressor processing (Humke et al., 2010) in a cilia-independent step (Jia et al., 2009), does not always cause phenotypes similar to pathway derepression from *Gpr161* deletion; for e.g., early embryonic deletion of *Sufu* in cerebellum does not exhibit Shh-subtype medulloblastoma formation (Kim et al., 2011) unlike *Gpr161* deletion (Shimada et al., 2018). However, studying the role of derepression of Shh signaling in forebrain development is important for understanding the basis of inverse repressive regulation of the Shh pathway.

Forebrain development requires close coordination between proliferation and differentiation of neuroepithelial cells and radial glia. Neuroepithelial cells are stem cells in the ventricular zone of the developing neocortex that divide symmetrically to expand the progenitor pool prior to the onset of neurogenesis. Starting from ~E11.5, neuroepithelial cells differentiate into progenitors called radial glia. Radial glia are neural stem cells that give rise to intermediate progenitor cells, neurons, glia and ependymal cells (Fuentealba et al., 2015; Gotz and Huttner, 2005; Kwan et al., 2012; Paridaen and Huttner, 2014; Spassky et al., 2005). Radial glia are bipolar in shape connecting the ventricular with the pial surface, and serve as a scaffold for neuronal migration (Borrell and Gotz, 2014; Rakic, 1972). Solitary primary cilia containing apical processes of the radial glia constitute the ventricular surface mostly during embryogenesis, whereas multiciliated ependymal cells cover the surface postnatally.

Although ependymal cells are derived from radial glia during embryogenesis, maturation of ependymal cells and formation of motile cilia occur later, during the first postnatal week (Spassky et al., 2005). The cerebrospinal fluid (CSF), which is produced by the choroid plexus that is also multiciliated, circulates within the brain ventricles before being absorbed into the blood in the sub-arachnoid space (Weller et al., 1992). The orchestrated beating of motile cilia on ependymal cells helps in CSF circulation (Ibanez-Tallon et al., 2004). Excessive accumulation of CSF in brain ventricles results in hydrocephalus, and affects 1 in 1000 infants in close association with disruption of brain structure, intellectual disability,

and developmental delays. Whereas abnormalities in ependymal cells and motile cilia have been well studied in hydrocephalus (Banizs et al., 2005; Ibanez-Tallon et al., 2004), the role of ventricular development prior to ependymal maturation in pathogenesis of hydrocephalus is not well understood.

Here, by conditionally deleting Gpr161, we describe the critical role of basal suppression of Shh pathway during early mid-gestation in regulating forebrain and ventricular architecture.

Materials and Methods

Mice

All protocols were approved by the UTSW Institutional Animal Care and Use Committee. Both male and female mice were analyzed. Mice were housed in standard cages with water and standard diet *ad libitum*, and 12 hour light/dark cycle. *Nestin-Cre* mice (Stock No. 003771) and *hGFAP-Cre* mice (Stock No. 004600) were obtained from Jackson Laboratory (Bar Harbor, ME) (Tronche et al., 1999; Zhuo et al., 2001) and $Gpr161^{fl/fl}$ mice were generated in house (Hwang et al., 2018; Shimada et al., 2018). All mice were backcrossed onto a C57BL/6J background for at least three generations prior to analysis. Control mice were a combination of $Gpr161^{fl/fl}$, $Gpr161^{fl/+}$, $Gpr161^{+/+}$ or *Nestin-Cre;* $Gpr161^{fl/+}$ mice. We did not observe any obvious phenotypic differences among mice with these genotypes. BrdU was injected i.p. (50 mg/kg in PBS) 1 h before dissections. Genotyping oligos are mentioned in Table S1 (Supplementary material). Sources of reagents are in Key resources table.

Tissue processing, antibodies, immunostaining and microscopy

Adult mouse brains were perfused with PBS and dissected for fixation in 4 % parafolmaldehyde overnight at 4°C. To fix embryonic and postnatal brains, the skin of mouse head was removed and an incision was done on the skull. The whole head was fixed in 4% parafolmaldehyde overnight at 4°C, and processed for cryosection or paraffin section. For cryosections, the samples were incubated in 30% sucrose for 1–2 days at 4°C, mounted with OCT compound, and cut into 15 μm frozen sections. The frozen sections were incubated in PBS for 15 min to dissolve away the OCT. Sections were then blocked in blocking buffer (3% normal donkey serum, 0.4% Triton X in PBS) for 1 h at room temperature. Sections were incubated overnight at room temperature with primary antibodies (Key resources table). After washes, the sections were incubated in secondary antibodies (1:500) for 1 h at room temperature. For Phallodin, sections were incubated with Phallodin conjugated with Alexa 568 for 1 hour at room temperature. Cell nuclei were stained with DAPI (Sigma). For BrdU staining, sections were treated with 2 N HCl for 15 min at 37°C, and washed before incubating with blocking buffer. For staining with antibodies against Pax6, Sox2 and Tbr2, sections were treated with 0.1 M citric acid (pH 6.0; pre-warmed to 60–70°C) and mil dly heated in a microwave (5 rounds of 20 seconds of microwave heating with 2 min and 40 seconds between rounds), followed by three PBS washes, prior to primary antibody incubation. Slides were mounted with Fluromount-G. For neocortical cytoarchitecture analysis, P0 brains were fixed with 4% PFA and transferred to 30% sucrose solution for 48 h at 4°C. Coronal sections (35 μm) were made using a SM2000

R sliding microtome (Leica) and free-floating sections were stored in PBS with 0.01% sodium azide at 4°C. Slices were washed thrice in TBS (10 mM Tris pH 8, 150 mM NaCl) for 5 min, and incubated for 30 min in 0.3 M Glycine in TBST (TBS with 0.4% Triton X-100). After rewashing, slices were incubated in primary antibody solution (TBST with 1% BSA, 3% normal donkey serum; see Key resources table for list of primary antibodies) overnight at 4°C. Next day, the slices were washed and incubated with secondary antibody solutions (AlexaFluor secondaries 1:1000 in TBST with 1% BSA, 3% normal donkey serum) for 1 h at room temperature. Slices were washed before mounting to microscope slides, protected from light, and allowed to dry before mounting coverslips using Prolong Diamond Antifade Mountant. Coverslips were allowed to dry overnight before confocal imaging. The images were acquired with a Zeiss LSM780 and LSM880 confocal microscopes.

In situ hybridization (ISH)

Whole-mount *in situ* hybridization using digoxigenin-labeled *Ptch1* probe (from Andrew McMahon's lab, University of Southern California) was performed on P0–4 SVZs using standard protocols. Images were acquired using a Leica stereomicroscope (M165 C) with digital camera (DFC500) (Mukhopadhyay et al., 2013). Radioisotopic in situ hybridization using anti-sense and sense *Gpr161* probes has been described before (Mukhopadhyay et al., 2013).

Quantitative RT-PCR and Immunoblotting

Quantitative RT-PCR was performed as before (Shimada et al., 2018). Primer sequences are in Table S1 (Supplementary material). Embryos were processed for Gli3 immunoblotting as described previously (Wen et al., 2010).

Scanning electron microscopy

The SVZs were dissected and then fixed in 2.5% glutaraldehyde in 0.1 M sodium cacodylate buffer overnight at 4°C. After three was hes in 0.1 M sodium cacodylate buffer, the samples were post-fixed with 2% osmium tetroxide in 0.1 M sodium cacodylate buffer for 2 hours. Samples were then dehydrated in ethanol, followed by critical point drying (Tousimis Samdri-795). Samples were air dried in a hood, mounted on SEM stubs, and sputter coated with gold/palladium using a Cressington 108 auto sputter coater. Images were acquired using a Field-Emission Scanning Electron Microscope (Zeiss Sigma) at 2–3 kV.

Cell quantification and statistics

The ventricular area of the lateral ventricle at P0 was quantified from 4–5 DAPI stained sections (150 μm apart) starting from posterior to the eye from 5 mice each using ImageJ, with only one side/mice being counted. The ventricular wall length of the lateral ventricle at E15.5 was quantified from 5–6 DAPI stained sections (150 μm apart) starting from just anterior to the eye from 3 mice each using ImageJ, with only one side/mice being counted. For cortex quantification from a "field" we averaged marker-positive cells from three images of different sections of the designated region from each mouse embryo or pup taken with 20× or 40× objectives in a LSM780 or LSM880. Data from 3–6 mice per genotype is shown.

The thickness of the cortex was measured manually using Image J from at least three sections per mouse. For neocortical cytoarchitectural analysis, 2–3 consecutive sections from each hemisphere were imaged and quantified at the indicated cortical region. Relative thickness of transcription factor-positive neurons was calculated as follows: An average of 10 serial quantifications normalized as a % of total neocortical thickness was calculated for one hemispherical section. Similar counts from 2–3 consecutive sections were averaged for calculating the relative thickness per hemisphere. For quantifying absolute number of respective transcription factor-positive neurons, neurons from three 50 μm squares in the indicated neocortical layers were counted per hemisphere. No blinding was performed. Sample sizes were based on our experience with these assays. To assess the statistical significance of differences among treatments we often performed unpaired, two-sided, student's *t* tests that assumed unequal variances in treatments. No mice or samples were excluded from any experiments. Microsoft Excel and GraphPad Prism (GraphPad, La Jolla, CA) were used for statistical analysis. Values of $p<0.05$ were considered significant.

Results

Lack of *Gpr161* in forebrain during mid-gestation causes hydrocephalus, periventricular heterotopia and polymicrogyria

We assessed *Gpr161* expression patterns in the embryonic brain by radioisotopic *in situ* hybridization. At E15.5, *Gpr161* transcript was broadly expressed in the whole forebrain and midbrain both dorsally and ventrally, including the cortex (Fig. 1A). Gpr161 also localized to the primary cilia of cortical radial glia projecting into the lateral ventricles (Fig. 1B). To test whether Gpr161 is required for brain development, we conditionally deleted *Gpr161* in nervous system using *Nestin-Cre* (Fig. 1C) (*Nestin-Cre; Gpr161*$^{fl/fl}$, hereafter referred to as *Nestin-Gpr161* cko), which is effective in initiating deletions starting from E10.5 (Mignone et al., 2004; Tronche et al., 1999). *Gpr161* transcripts were fully depleted in the cortex at E14.5 (Fig. 1D).

Phenotypic characterization of these mice revealed that *Nestin-Gpr161* cko mice had domed heads (Fig. 1E) due to enlarged lateral ventricles (ventriculomegaly) at post-natal day 0 (P0), which developed into full-blown hydrocephalus (Fig. 1F, 1G, Supplementary movies 1–4) before death at 5–6 months. The expansion of lateral ventricular wall extended into the subependymal layer in the olfactory bulb (Fig. 1F, arrows). These mice also suffered from cerebellar dysplasia and Shh-subtype medulloblastoma (Shimada et al., 2018). Remarkably, *Nestin-Gpr161* cko mice also developed excessive folding in the rostral cingulate cortex (polymicrogyria) (Fig. 1H, 1I). In addition, *Nestin-Gpr161* cko mice had periventricular heterotopia as marked by heterotopic cell clusters adjacent to the lateral ventricle (Fig. 1H, 1J).

Late midgestational deletion of *Gpr161* does not grossly affect the forebrain.

In contrast to *Nestin-Gpr161* cko, deletion of *Gpr161* using *hGFAP-Cre* (*GFAP-Gpr161* cko) (Fig. 1C) in all multipotent progenitors of the dorsal forebrain starting from E13.5 (Garcia et al., 2004; Ohata et al., 2014; Zhuo et al., 2001) did not result in hydrocephalus and periventricular heterotopia (Fig. 2A–B). In the cerebellar anlage, *hGFAP-Cre*-mediated

recombination occurs in the proliferating progenitors in the ventricular zone, and upper rhombic lip that ultimately give rise to granule progenitors (Spassky et al., 2008). In contrast to forebrain that had no apparent phenotypes, *GFAP-Gpr161* cko developed cerebellar dysplasia (Fig. 2A) and Shh-subtype medulloblastomas, as reported before (Shimada et al., 2018). Neither *Nestin-Gpr161* cko nor *GFAP-Gpr161* cko animals had ciliary defects as apparent from Arl13b immunostaining for radial glial lining the lateral ventricles (Fig. 2C–D). Thus, Gpr161 is critical in radial glia and their derivatives for proper forebrain development during early mid-gestational period.

Gpr161 deletion causes hydrocephalus despite lack of ependymal cell or aqueductal defects

Hydrocephalus can be caused by blockage of cerebrospinal fluid (CSF) flow (Banizs et al., 2005), reduced absorption of CSF at arachnoid granulations, defects in ependymal cell differentiation and maturation (Shimada et al., 2017) or defects in motile cilia movement (Ibanez-Tallon et al., 2004). To understand the formation of hydrocephalus in *Nestin-Gpr161* cko mice, we analyzed multicilia of ependymal cells. Interestingly, we did not find any structural defects of ependymal cilia on the lateral ventricle of *Nestin-Gpr161* cko mice at 2 months of age by scanning electron microscope (SEM) at different areas (Fig. 3A, 3B,S1A and S1B). Maturation of multiciliated ependymal cells happens during the first two weeks of postnatal life, and this time window is critical for hydrocephalus formation (Spassky et al., 2005). Notably, we did not find any differences in basal body multiplication during ependymal cell differentiation on the lateral wall of the lateral ventricle at P7 (Fig. 3C, 3D). We also did not observe abnormal expression levels of transcription factors that are critical for ependymal cell differentiation in the cortex at E14.5 and subventricular zone (SVZ) at P0 (Fig. 3E, 3F). To examine whether the aqueductal stenosis contributes to hydrocephalus, we examined the aqueductal morphology of *Nestin-Gpr161* cko mice at P0 rostrocaudally, but found no difference between experimental groups (Fig. 3G, 3H). These data indicate that ependymal cell development and multicilia formation were unaffected and could not account for hydrocephalus formation of *Nestin-Gpr161* cko mice.

Derepression of Shh signaling throughout *Gpr161* cko telencephalon

The surface areas of the apical domains of radial glia are enlarged in a primary cilia deleted mouse model during late embryogenesis causing postnatal hydrocephalus (Foerster et al., 2017). Therefore, we analyzed the apical processes of radial glia in *en face* view of the cortex at E14.5. The number of apical domains of radial glia per unit area did not significantly differ between *Nestin-Gpr161* cko mice and littermate controls (Fig. 4A, 4B), suggesting that unlike ciliary loss, dysregulation of the apical process surface area was not causing hydrocephalus.

As Gpr161 negatively regulates Shh pathway during neural tube formation, we analyzed Shh signaling in the embryonic cortex at E14.5 and SVZ at P0. Shh pathway transcripts were highly upregulated in the cortex and SVZ of *Nestin-Gpr161* cko mice as compared to the littermate controls (Fig. 4C, 4D). Similarly, the lateral ventricular surface area was significantly enlarged at P0 (Fig. 1G), and there was dorsoventral expansion of Shh pathway activity as detected by *Ptch1* RNA *in situ* hybridization (Fig. 4E). Gli3 full-length levels

were unaffected upon immunoblotting, whereas Gli3 repressor levels trended towards reduction in the E14.5 cortex (Fig. 4F–H). Thus, overall Shh pathway activity is upregulated throughout the telencephalon upon *Gpr161* deletion.

Ventriculomegaly in mid-gestation *Nestin-Gpr161* cko embryos is associated with increased radial glial proliferation

As we detected increased ventricular size at P0 (Fig. 1G, 4E), we further probed the developmental window for occurrence of ventriculomegaly. By E13.5, we detected increased surface area of the lateral ventricles anteriorly, although dorsal telencephalic midline structures such as the cortical hem and choroid plexus were unaffected (Fig. 5A, S2A, Supplementary movies 5–7). The increased size of lateral ganglionic eminences (LGEs) and the dorsolateral wall of the lateral ventricles were clearly apparent at E15.5 along with a more conical shape of the ventricular roof and increased wall length (Fig. 5B and 5D). Dorsoventral patterning was not grossly affected, as Pax6 and Mash1 positive progenitors persisted in dorsal and ventral walls of the lateral ventricles, respectively, suggesting that high Shh signaling in the telencephalon did not cause disruption of patterning (Fig. 5C). However, we noted an increase in proliferation of the radial glia in the MGEs, and a trend towards a similar increase in the LGEs by pH3 immunostaining (Fig. 5E, 5F, 5G) as early as E13.5. However, such increases were not apparent in the cortex at E13.5 (Fig. S2B and S2C) or in the SVZ at later stages (E15.5) (Fig. S2D–F). Thus, an increase in proliferation and total number of radial glia in the lateral ventricles in early mid-gestational ages might contribute to the increase in lateral ventricular surface area causing ventriculomegaly preceding postnatal hydrocephalus.

Gpr161 deletion expands intermediate progenitors and basal radial glia in cortex

Radial glia proliferate and generate neurons in the cortex during embryogenesis. Apical radial glia (aRG) divide at the cortical ventricular surface (VZ) and differentiate into intermediate progenitor cells (IPCs) in the SVZ in the cortex. Another type of radial glia called basal radial glia (bRG) is localized in the intermediate zone (IZ) and is unipolar with connection only to the pia. bRG undergo mitosis in the IZ and play a role in gyrus formation (Paridaen and Huttner, 2014; Sun and Hevner, 2014). We examined the role of Gpr161 in regulation of radial glia during corticogenesis in lateral and medial regions (Fig. 6A). The total number of Pax6-positive aRG did not significantly differ between *Nestin-Gpr161* cko mice and littermate controls at E15.5 (Fig. 6B–C). Notably, Tbr2-positive IPCs were significantly increased in *Nestin-Gpr161* cko mice at E15.5 both laterally and medially (Fig. 6B, 6D). Interestingly, the number of bRG (Pax6-positive and Tbr2-negative cells outside of the VZ) was significantly increased in *Nestin-Gpr161* cko mice (Fig. 6B, 6E). These data indicate that the fate of radial glia is switched to increased neurogenesis and bRG formation following *Gpr161* deletion throughout the developing cortex. We did not detect any difference in the number of apoptotic cells at E15.5 (Fig. 6I). In agreement with the increased number of IPCs, the number of mitotic cells in the SVZ and IZ (but not in the VZ) as measured by pH3 immunostaining, was increased in *Nestin-Gpr161* cko mice at E15.5 (Fig. 6F–H). Thus, both IPC and bRG proliferation is increased in E15.5 *Nestin-Gpr161* cko cortex.

Gpr161 deletion regulates cortical lamination

To assess the outcome of increased neurogenesis at E15.5, we analyzed the cortex at P0. Although polymicrogyria was observed in the medial cingulate cortex in *Nestin-Gpr161* cko mice (Fig. 1H and 1I), the cortex was significantly thinner laterally as compared to littermate controls (Fig. 7B). The number of Pax6-positive aRG was also decreased in *Nestin-Gpr161* cko mice as compared to littermate controls (Fig. 7C and 7D). In agreement with published data (Wang et al., 2011), increased generation of IPCs (Fig. 6D) and bRG (Fig. 6E) results in depletion of aRG at the expense of aRG maintenance.

As *Nestin-Gpr161* cko mice demonstrated defects in cortical radial glial differentiation and maintenance, we tested for lamination in the lateral regions of the neocortex (Fig. 7A) by examining the expression of known neocortical layer markers. We immunostained for deep layer markers Tbr1 and Ctip2, and upper layer markers Satb2 and FoxP1 at P0 (Greig et al., 2013; Popovitchenko and Rasin, 2017). The thickness of Tbr1 or Ctip2 positive layers relative to the neocortex were significantly reduced in *Nestin-Gpr161* cko compared to control (Fig. 7E–F). However, the relative thickness of Satb2 positive layer was increased, while the FoxP1 positive layer trended to be thicker but was not significantly different in *Nestin-Gpr161* cko (Fig. 7E–F) compared to controls. The density of Tbr1 positive deep-layer neurons was decreased, whereas Satb2 positive neurons in layer II were significantly denser compared to controls (Fig. 7E, G). The cingulate cortex showed folding of cortex with Satb2 and FoxP1 positive neurons in the polymicrogyric region (Fig. 7H). Thus, lack of Gpr161 during early mid-gestation causes altered neocortical cytoarchitecture.

Deletion of *Gpr161* results in periventricular nodular heterotopia from neuron-intrinsic migration defects

By following the periventricular heterotopia into adulthood, we noted accumulating nodules at 6 months in the lateral ventral ventricular walls (Fig. 8A). The nodules were positive for neuronal marker, NeuN at P14 (Fig. 8B). The nodules lacked progenitor markers such as Sox2, the astrocyte marker GFAP and proliferation markers, but expressed doublecortin, suggesting preponderance of differentiating neuronal cells and without much proliferation (Fig. 8C–8E). To address the developmental requirement for Gpr161 in neural stem cell function in the lateral ventricles, we also analyzed neural stem cells in the SVZ of *Nestin-Gpr161* cko mice at P0. Notably, while *Gpr161* mRNA was significantly decreased in the SVZ of *Nestin-Gpr161* cko mice at P0 (Fig. 9A), there was clear accumulation of NeuN positive nodules in the SVZ at P0 (Fig. 9B), with increased thickness (Fig. 9C). Apical anchoring of cells lining the ventricles in SVZ was not disrupted at P0 as examined by phalloidin staining (Fig. 9D) (Feng et al., 2006), neither were cell-cell contacts affected as determined by bcatenin immunostaining (Fig. 9E). The radial glial fibers were also unperturbed, even in heterotopic areas, in the *Nestin-Gpr161* cko (Fig. 9F, 9G). Notably, accumulation of doublecortin-positive differentiating neurons was observed in the SVZ of *Nestin-Gpr161* cko mice at P0 (Fig. 9H). Thus, the periventricular nodular heterotopia in *Nestin-Gpr161* cko mice occurred in the absence of defects in either integrity of apical processes or the glial scaffold, likely resulting from disrupted neuronal migration and accumulation of differentiating neurons.

Discussion

Basal suppression of Shh pathway in telencephalon

The physiological role of primary cilia-generated signaling and basal suppression of the Shh pathway in forebrain and ventricular development is unclear. Here, we demonstrate that active repression of the Shh pathway by the primary cilia localized GPCR, Gpr161 is critical in forebrain architecture and ventricular homeostasis. Derepression of Shh signaling upon deletion of *Gpr161* in developing forebrain during mid-gestation causes ventriculomegaly preceding postnatal hydrocephalus, and without affecting ependymal cells. The ventricular surface expansion is apparent by late mid-gestation from increased radial glial proliferation in the ganglionic eminences. Increased intermediate progenitor cell and basal radial glia are associated with region-specific effects in the cortex, including lateral cortical thinness, altered neocortical cytoarchitectonic structure, and increased gyration in cingulate cortex. Furthermore, disruption of periventricular neuronal migration without affecting the glial scaffold causes periventricular nodular heterotopia. Overall, Gpr161 functions as a rheostat repressing Shh signaling and regulating ventricular and periventricular development in the forebrain (Fig. 10A).

Ventriculomegaly causes hydrocephalus

Ventriculomegaly primarily contributes to hydrocephalus in *Nestin-Gpr161* cko, as ependymal cell differentiation and maturation to multiciliated cells, or aqueductal morphology remain unaffected. Ventriculomegaly is evident as early as E13.5. Increased Shh signaling during early mid-gestation is the likely mechanism underlying the ventriculomegaly in *Nestin-Gpr161* cko for the following reasons. First, *Gpr161* deletion in forebrain mimics features such as expansion of LGE/MGE in *Shh* mutants lacking in cholesterol modification (*ShhN*/+) with long range and ectopic pathway activity (Himmelstein et al., 2010; Huang et al., 2007) or extraneous expression of Shh (Komada et al., 2008; Shikata et al., 2011). However, *Nestin-Gpr161* cko does not completely lack dorsal telencephalic structures such as cortical hem, as seen in *ShhN*/+ embryos (Himmelstein et al., 2010) that might arise from higher regional ectopic Shh pathway activity. Similarly, the neocortex, medial pallium and the ganglionic eminences are disorganized at E14.5 in *Nestin-cre; Ptch1*$^{f/f}$ (*Nestin-Ptch1* cko) mice, which are E15.5 lethal. The ventricular surface in *Nestin-Ptch1* cko is extensively irregular and folded suggesting ventriculomegaly (Dave et al., 2011). Second, deletion of *Sufu* at midgestation in cortical neuroprogenitors using *Emx1-Cre* (*Emx1-Sufu* cko) results in disrupted dorsal forebrain development and ventriculomegaly (Yabut et al., 2015). However, deletion of *Sufu* using *hGFAP-Cre* (*GFAP-Sufu* cko) does not result in ventriculomegaly (Yabut et al., 2016). Similarities in ventriculomegaly between *Nestin-Gpr161* cko and *Emx1-Sufu* cko models suggest that a critical level of high Shh signaling in neuroepithelial cells and radial glia during early neurogenesis is important for causing these phenotypes. Finally, *Gli2/3* double knockouts are also embryonic lethal by E13 with the ventral telencephalon being highly disorganized, and difficult to interpret (Yu et al., 2009). *NestinCre; Gli3*$^{f/Xt}$ conditional knockouts in radial glia cause abnormal specification of ependymal lineage, but have no hydrocephalus (Wang et al., 2014). Deletion of *Gli3* does not cause Shh pathway derepression (Wang et al., 2014;

Yu et al., 2009) unlike *Nestin-Gpr161* cko, again suggesting a critical level of high Shh signaling required for ventriculomegaly formation in the latter (Fig. 10B).

Defects in radial glial cilia and ciliary signaling might underlie multiple brain abnormalities in ciliopathy syndromes, such as Joubert and related syndromes (Bielas et al., 2009; Cantagrel et al., 2008; Higginbotham et al., 2012; Higginbotham et al., 2013). However, the mechanisms underlying the role of cilia in dorsal forebrain patterning have been controversial. Loss of cilia using a homozygous hypomorphic allele of the ciliary intraflagellar transport-B (IFT-B) complex component *Ift88* (*Ift88*^{cbl}) has been reported to result in larger brains at birth, and disorganization of telencephalic structures (Willaredt et al., 2008). Similarly, lack of the ciliary anterograde kinesin II, Kif3a (*Nestin-Cre; Kif3a*$^{f/f}$) showed ventriculomegaly, and larger cortices with irregular thickness and ventricular surface invaginations by E13.5 (Wilson et al., 2012). Both models have increased levels of the Shh pathway target, *Ptch1* ventrally but not expanding dorsally, suggesting moderate pathway activity, unlike *Gpr161* loss. Multiple factors contribute to ventriculomegaly upon cilia loss such as increased size of apical radial glial processes (Foerster et al., 2017), or choroid plexus ciliary abnormalities associated with oversecretion of CSF (Banizs et al., 2005), neither of which were present in *Nestin-Gpr161* cko.

Rather, the increase in ventricular surface in mid-gestation in in *Nestin-Gpr161* cko is likely due to the total increase of radial glial populations from increased proliferation as seen in ganglionic eminences at E13.5. In the developing chick neural tube, Shh signaling promotes symmetrical cell divisions in motor neuron progenitors (Saade et al., 2017; Saade et al., 2013). Upregulation of pericentrin from Shh signaling in these progenitors causes centrosomal recruitment of PKA regulatory subunit II (PKA-RII) and PKA catalytic subunits in promoting symmetric cell divisions. Unlike PKA's role as a negative regulator of Shh signaling during neural tube patterning (Tuson et al., 2011), the recruitment of PKA to centrosomes upon high Shh signaling suggests a parallel and positive role of PKA in promoting Shh-dependent neuroprogenitor proliferation. Upregulation of Shh signaling in *Nestin-Gpr161* cko radial glia during early mid-gestation could promote proliferation by similar mechanisms. Other factors such as dysregulated neuroepithelial cell to radial glia transition (Caviness et al., 1995; Rakic, 1995; Sahara and O'Leary, 2009) and abnormal cell cycle exit of neuroprogenitors (Caviness et al., 2003; Chenn and Walsh, 2002) could also affect cortical and ventricular growth and could be regulated by high Shh signaling during mid-gestation. Overall, ventriculomegaly in the *Nestin-Gpr161* cko model firmly establishes ventricular expansion during embryogenesis in causation of hydrocephalus, independent of primary or motile ciliary morphology defects.

Polymicrogyria and cortical lamination defects in *Nestin-Gpr161* cko

The increase in IPCs and basal radial glia in the cortex in both lateral and medial regions at later gestational ages, and the cingulate cortex polymicrogyria upon *Gpr161* deletion is similar to *GFAP-Cre; SmoM2* mice (*GFAP-SmoM2* cko) or *Nestin-Cre; SmoM2* (*Nestin-SmoM2* cko) mice (Wang et al., 2016). However, unlike the *SmoM2* expressing mice, thinning of the cortex with a reduction of total Pax6-positive aRGs by P0 was observed, possibly arising from gradual depletion of neurogenesis among radial glial progenitors

resulting from earlier deletion in *Nestin-Gpr161* cko versus *GFAP-SmoM2* cko. Increased folding in *GFAP-SmoM2* cko has been correlated with cortical lamination defects with increased upper layer and decreased deep layer neurons selectively in the medial and cingulate cortex regions (Wang et al., 2016), but not in the lateral cortex (Yabut et al., 2015). However, *Nestin-Gpr161* cko has similar cortical lamination defects in the lateral cortex, but less severe polymicrogyria, suggesting additional or alternative mechanisms. Rather, increased folding of the cortex might be related to IPC populations, as seen in mice with transgenic overexpression of human *Gpr56* that regulates gyral patterning (Bae et al., 2014). *GFAP-Sufu* cko show an expansion of IPCs (Yabut et al., 2016), whereas *Emx1-Sufu* cko shows a decrease (Yabut et al., 2015). *NestinCre; Gli3*$^{f/Xt}$ conditional knockouts reduce IPC production at E18.5 (Wang et al., 2011); however, *Emx1-Cre; Gli3*$^{f/f}$ mice (*Emx1-Gli3* cko) have variable IPC levels, with reduced production at E11.5 and higher production at E12.5 (Hasenpusch-Theil et al., 2018) (Fig. 10B). However, polymicrogyria has not been reported in either *Sufu* or *Gli3* cko models, unlike *Nestin-Gpr161* cko or *SmoM2* expressing mice, highlighting the importance of studying Shh pathway derepression using multiple model systems to unravel important phenotypes and also reexamining these existing models for polymicrogyria.

Unlike *Nestin-Gpr161* cko, neocortical cytoarchitecture was severely disorganized in *Emx1-Sufu* cko and *Emx1-SmoM2* cko, where both upper and deep layer neurons were distributed throughout neocortex along with a deficient production of upper cortical layer neurons (Yabut et al., 2015). *GFAP-Sufu* cko was grossly indistinguishable from control littermates and caused only mild increase in Cux1-positive neurons in layer 4 (Yabut et al., 2016) (Fig. 10B). Rather, the decrease in neocortical deep layer neurons and increase in upper layer neurons in *Nestin-Gpr161* cko is similar to some extent with *Emx1-Gli3* cko (Hasenpusch-Theil et al., 2018) mice, although with lesser expansion of upper layers (Fig. 10B). In *Emx1-Gli3* cko, reduced deep layer formation is preceded by a decrease in G1/S phase of radial glial cell cycle (Hasenpusch-Theil et al., 2018). Similarly, in mice deficient for the cell cycle inhibitor p27^{kip1} (p27), decreased exit from cell cycle in radial glia during neocortical development is correlated with increased upper layers with respect to deep layer neurons (Caviness et al., 2003) similar to *Nestin-Gpr161* cko, but with overall increase in neocortical thickness. Thus, the neocortical cytoarchitectonic structural phenotypes in *Nestin-Gpr161* cko could be related to altered cell cycle properties of radial glial during particular phases of cortical neuron formation.

Periventricular heterotopia upon *Gpr161* deletion

A common genetic mutation in periventricular heterotopia is in the F-actin-binding cytoplasmic crosslinking phosphoprotein *Filamin A (FLNA)* gene. Disorganization of radial glia (Carabalona et al., 2012), defective neuronal migration (Sarkisian et al., 2006), defective contacts between apical radial glial processes (Feng et al., 2006), and gradual defects in the neuroependymal lining (Ferland et al., 2009) have been shown to contribute to periventricular heterotopia. However, in the *Nestin-Gpr161* cko mice, we do not see defects in the neuroepithelial lining during embryonic stages. *Arl13b*^{hnn} mice lacking in Arl13b (Caspary et al., 2007), a small GTPase that regulates lipidated cargo trafficking to cilia (Gotthardt et al., 2015) develop cortical heterotopia from disruption of the radial glia

scaffold caused by aberrant development of radial progenitors (Higginbotham et al., 2013). However, in *Nestin-Gpr161* cko mice the radial glial scaffold was not affected. Rather, the periventricular heterotopia most likely stems from neuron-intrinsic migration defects and ectopic accumulation of differentiating neurons from high Shh signaling during early mid-gestation. Patients with periventricular heterotopia associated with limb abnormalities or hydrocephalus but not having mutations in *FLNA* have been reported (Parrini et al., 2006). As dysregulated Shh signaling regulates both skeletal morphogenesis (Hwang et al., 2018) and hydrocephalus (this study), mutations in *GPR161* or in genes encoding other members of the *SHH* pathway could contribute to pathogenesis in some of these cases.

Conclusion

Nestin-Gpr161 cko-specific phenotypes such as ventriculomegaly-induced hydrocephalus, polymicrogyria and periventricular heterotopia likely arise from a critical level of high Shh pathway activity in forebrain during early mid-gestation. Derepression of Shh signaling could prolong radial glial proliferation versus differentiation in midgestation, increase intermediate progenitor cell and basal radial glial production contributing to these phenotypes.

Supplementary Material

Refer to Web version on PubMed Central for supplementary material.

Acknowledgements

We thank Drs. Maria Chahrour and Sandra Schmid for comments on the manuscript. We thank Dr. Marcel Mattlen, Dr. Robert Hammer and the Mouse Transgenic Core, Live Cell Imaging Facility, and the Molecular Pathology Core at UT Southwestern.

Funding

This work was supported by the Alex's Lemonade Foundation (an A-grant to S.M.), Welch Foundation (grant #I-1906 to SM), and National Institutes of Health (grant #1R01GM113023 to S.M., and S10RR029731 to Live Cell Imaging Facility, UT Southwestern).

References

Ashe HL, Briscoe J, 2006 The interpretation of morphogen gradients. Development 133, 385–394. [PubMed: 16410409]

Bachmann VA, Mayrhofer JE, Ilouz R, Tschaikner P, Raffeiner P, Rock R, Courcelles M, Apelt F, Lu TW, Baillie GS, Thibault P, Aanstad P, Stelzl U, Taylor SS, Stefan E, 2016 Gpr161 anchoring of PKA consolidates GPCR and cAMP signaling. Proc Natl Acad Sci U S A 113, 7786–7791. [PubMed: 27357676]

Bae BI, Tietjen I, Atabay KD, Evrony GD, Johnson MB, Asare E, Wang PP, Murayama AY, Im K, Lisgo SN, Overman L, Sestan N, Chang BS, Barkovich AJ, Grant PE, Topcu M, Politsky J, Okano H, Piao X, Walsh CA, 2014 Evolutionarily dynamic alternative splicing of GPR56 regulates regional cerebral cortical patterning. Science 343, 764–768. [PubMed: 24531968]

Bai CB, Joyner AL, 2001 Gli1 can rescue the in vivo function of Gli2. Development 128, 5161–5172. [PubMed: 11748151]

Banizs B, Pike MM, Millican CL, Ferguson WB, Komlosi P, Sheetz J, Bell PD, Schwiebert EM, Yoder BK, 2005 Dysfunctional cilia lead to altered ependyma and choroid plexus function, and result in the formation of hydrocephalus. Development 132, 5329–5339. [PubMed: 16284123]

Bielas SL, Silhavy JL, Brancati F, Kisseleva MV, Al-Gazali L, Sztriha L, Bayoumi RA, Zaki MS, Abdel-Aleem A, Rosti RO, Kayserili H, Swistun D, Scott LC, Bertini E, Boltshauser E, Fazzi E, Travaglini L, Field SJ, Gayral S, Jacoby M, Schurmans S, Dallapiccola B, Majerus PW, Valente EM, Gleeson JG, 2009 Mutations in INPP5E, encoding inositol polyphosphate-5-phosphatase E, link phosphatidyl inositol signaling to the ciliopathies. Nat Genet 41, 1032–1036. [PubMed: 19668216]

Blaess S, Corrales JD, Joyner AL, 2006 Sonic hedgehog regulates Gli activator and repressor functions with spatial and temporal precision in the mid/hindbrain region. Development 133, 1799–1809. [PubMed: 16571630]

Borrell V, Gotz M, 2014 Role of radial glial cells in cerebral cortex folding. Current opinion in neurobiology 27, 39–46. [PubMed: 24632307]

Cantagrel V, Silhavy JL, Bielas SL, Swistun D, Marsh SE, Bertrand JY, Audollent S, Attie-Bitach T, Holden KR, Dobyns WB, Traver D, Al-Gazali L, Ali BR, Lindner TH, Caspary T, Otto EA, Hildebrandt F, Glass IA, Logan CV, Johnson CA, Bennett C, Brancati F, International Joubert Syndrome Related Disorders Study, G., Valente EM, Woods CG, Gleeson JG, 2008 Mutations in the cilia gene ARL13B lead to the classical form of Joubert syndrome. Am J Hum Genet 83, 170–179. [PubMed: 18674751]

Carabalona A, Beguin S, Pallesi-Pocachard E, Buhler E, Pellegrino C, Arnaud K, Hubert P, Oualha M, Siffroi JP, Khantane S, Coupry I, Goizet C, Gelot AB, Represa A, Cardoso C, 2012 A glial origin for periventricular nodular heterotopia caused by impaired expression of Filamin-A. Hum Mol Genet 21, 1004–1017. [PubMed: 22076441]

Caspary T, Larkins CE, Anderson KV, 2007 The graded response to Sonic Hedgehog depends on cilia architecture. Dev Cell 12, 767–778. [PubMed: 17488627]

Caviness VS Jr., Goto T, Tarui T, Takahashi T, Bhide PG, Nowakowski RS, 2003 Cell output, cell cycle duration and neuronal specification: a model of integrated mechanisms of the neocortical proliferative process. Cereb Cortex 13, 592–598. [PubMed: 12764033]

Caviness VS Jr., Takahashi T, Nowakowski RS, 1995 Numbers, time and neocortical neuronogenesis: a general developmental and evolutionary model. Trends Neurosci 18, 379–383. [PubMed: 7482802]

Chenn A, Walsh CA, 2002 Regulation of cerebral cortical size by control of cell cycle exit in neural precursors. Science 297, 365–369. [PubMed: 12130776]

Dave RK, Ellis T, Toumpas MC, Robson JP, Julian E, Adolphe C, Bartlett PF, Cooper HM, Reynolds BA, Wainwright BJ, 2011 Sonic hedgehog and notch signaling can cooperate to regulate neurogenic divisions of neocortical progenitors. PloS one 6, e14680. [PubMed: 21379383]

De Robertis EM, 2006 Spemann's organizer and self-regulation in amphibian embryos. Nat Rev Mol Cell Biol 7, 296–302. [PubMed: 16482093]

Feng Y, Chen MH, Moskowitz IP, Mendonza AM, Vidali L, Nakamura F, Kwiatkowski DJ, Walsh CA, 2006 Filamin A (FLNA) is required for cell-cell contact in vascular development and cardiac morphogenesis. Proc Natl Acad Sci U S A 103, 19836–19841. [PubMed: 17172441]

Ferland RJ, Batiz LF, Neal J, Lian G, Bundock E, Lu J, Hsiao YC, Diamond R, Mei D, Banham AH, Brown PJ, Vanderburg CR, Joseph J, Hecht JL, Folkerth R, Guerrini R, Walsh CA, Rodriguez EM, Sheen VL, 2009 Disruption of neural progenitors along the ventricular and subventricular zones in periventricular heterotopia. Hum Mol Genet 18, 497–516. [PubMed: 18996916]

Foerster P, Daclin M, Asm S, Faucourt M, Boletta A, Genovesio A, Spassky N, 2017 mTORC1 signaling and primary cilia are required for brain ventricle morphogenesis. Development 144, 201–210. [PubMed: 27993979]

Fuentealba LC, Rompani SB, Parraguez JI, Obernier K, Romero R, Cepko CL, Alvarez-Buylla A, 2015 Embryonic Origin of Postnatal Neural Stem Cells. Cell 161, 1644–1655. [PubMed: 26091041]

Garcia AD, Doan NB, Imura T, Bush TG, Sofroniew MV, 2004 GFAP-expressing progenitors are the principal source of constitutive neurogenesis in adult mouse forebrain. Nat Neurosci 7, 1233–1241. [PubMed: 15494728]

Goetz SC, Anderson KV, 2010 The primary cilium: a signalling centre during vertebrate development. Nat Rev Genet 11, 331–344. [PubMed: 20395968]

Gotthardt K, Lokaj M, Koerner C, Falk N, Giessl A, Wittinghofer A, 2015 A G-protein activation cascade from Arl13B to Arl3 and implications for ciliary targeting of lipidated proteins. Elife 4.

Gotz M, Huttner WB, 2005 The cell biology of neurogenesis. Nat Rev Mol Cell Biol 6, 777–788. [PubMed: 16314867]

Greig LC, Woodworth MB, Galazo MJ, Padmanabhan H, Macklis JD, 2013 Molecular logic of neocortical projection neuron specification, development and diversity. Nat Rev Neurosci 14, 755–769. [PubMed: 24105342]

Hasenpusch-Theil K, West S, Kelman A, Kozic Z, Horrocks S, McMahon AP, Price DJ, Mason JO, Theil T, 2018 Gli3 controls the onset of cortical neurogenesis by regulating the radial glial cell cycle through Cdk6 expression. Development 145.

Higginbotham H, Eom TY, Mariani LE, Bachleda A, Hirt J, Gukassyan V, Cusack CL, Lai C, Caspary T, Anton ES, 2012 Arl13b in primary cilia regulates the migration and placement of interneurons in the developing cerebral cortex. Dev Cell 23, 925–938. [PubMed: 23153492]

Higginbotham H, Guo J, Yokota Y, Umberger NL, Su CY, Li J, Verma N, Hirt J, Ghukasyan V, Caspary T, Anton ES, 2013 Arl13b-regulated cilia activities are essential for polarized radial glial scaffold formation. Nat Neurosci 16, 1000–1007. [PubMed: 23817546]

Himmelstein DS, Bi C, Clark BS, Bai B, Kohtz JD, 2010 Balanced Shh signaling is required for proper formation and maintenance of dorsal telencephalic midline structures. BMC Dev Biol 10, 118. [PubMed: 21114856]

Huang X, Litingtung Y, Chiang C, 2007 Ectopic sonic hedgehog signaling impairs telencephalic dorsal midline development: implication for human holoprosencephaly. Hum Mol Genet 16, 1454–1468. [PubMed: 17468181]

Humke EW, Dorn KV, Milenkovic L, Scott MP, Rohatgi R, 2010 The output of Hedgehog signaling is controlled by the dynamic association between Suppressor of Fused and the Gli proteins. Genes & development 24, 670–682. [PubMed: 20360384]

Hwang SH, White KA, Somatilaka BN, Shelton JM, Richardson JA, Mukhopadhyay S, 2018 The G protein-coupled receptor Gpr161 regulates forelimb formation, limb patterning and skeletal morphogenesis in a primary cilium-dependent manner. Development 145.

Ibanez-Tallon I, Pagenstecher A, Fliegauf M, Olbrich H, Kispert A, Ketelsen UP, North A, Heintz N, Omran H, 2004 Dysfunction of axonemal dynein heavy chain Mdnah5 inhibits ependymal flow and reveals a novel mechanism for hydrocephalus formation. Hum Mol Genet 13, 2133–2141. [PubMed: 15269178]

Jia J, Kolterud A, Zeng H, Hoover A, Teglund S, Toftgard R, Liu A, 2009 Suppressor of Fused inhibits mammalian Hedgehog signaling in the absence of cilia. Dev Biol 330, 452–460. [PubMed: 19371734]

Kim JJ, Gill PS, Rotin L, van Eede M, Henkelman RM, Hui CC, Rosenblum ND, 2011 Suppressor of fused controls mid-hindbrain patterning and cerebellar morphogenesis via GLI3 repressor. J Neurosci 31, 1825–1836. [PubMed: 21289193]

Komada M, Saitsu H, Kinboshi M, Miura T, Shiota K, Ishibashi M, 2008 Hedgehog signaling is involved in development of the neocortex. Development 135, 2717–2727. [PubMed: 18614579]

Kwan KY, Sestan N, Anton ES, 2012 Transcriptional co-regulation of neuronal migration and laminar identity in the neocortex. Development 139, 1535–1546. [PubMed: 22492350]

Mignone JL, Kukekov V, Chiang AS, Steindler D, Enikolopov G, 2004 Neural stem and progenitor cells in nestin-GFP transgenic mice. J Comp Neurol 469, 311–324. [PubMed: 14730584]

Mukhopadhyay S, Rohatgi R, 2014 G-protein-coupled receptors, Hedgehog signaling and primary cilia. Semin Cell Dev Biol 33, 63–72. [PubMed: 24845016]

Mukhopadhyay S, Wen X, Ratti N, Loktev A, Rangell L, Scales SJ, Jackson PK, 2013 The ciliary G-protein-coupled receptor Gpr161 negatively regulates the Sonic hedgehog pathway via cAMP signaling. Cell 152, 210–223. [PubMed: 23332756]

Ohata S, Nakatani J, Herranz-Perez V, Cheng J, Belinson H, Inubushi T, Snider WD, Garcia-Verdugo JM, Wynshaw-Boris A, Alvarez-Buylla A, 2014 Loss of Dishevelleds disrupts planar polarity in ependymal motile cilia and results in hydrocephalus. Neuron 83, 558–571. [PubMed: 25043421]

Paridaen JT, Huttner WB, 2014 Neurogenesis during development of the vertebrate central nervous system. EMBO Rep 15, 351–364. [PubMed: 24639559]

Parrini E, Ramazzotti A, Dobyns WB, Mei D, Moro F, Veggiotti P, Marini C, Brilstra EH, Dalla Bernardina B, Goodwin L, Bodell A, Jones MC, Nangeroni M, Palmeri S, Said E, Sander JW, Striano P, Takahashi Y, Van Maldergem L, Leonardi G, Wright M, Walsh CA, Guerrini R, 2006 Periventricular heterotopia: phenotypic heterogeneity and correlation with Filamin A mutations. Brain 129, 1892–1906. [PubMed: 16684786]

Popovitchenko T, Rasin MR, 2017 Transcriptional and Post-Transcriptional Mechanisms of the Development of Neocortical Lamination. Front Neuroanat 11, 102. [PubMed: 29170632]

Rakic P, 1972 Mode of cell migration to the superficial layers of fetal monkey neocortex. J Comp Neurol 145, 61–83. [PubMed: 4624784]

Rakic P, 1995 A small step for the cell, a giant leap for mankind: a hypothesis of neocortical expansion during evolution. Trends Neurosci 18, 383–388. [PubMed: 7482803]

Saade M, Gonzalez-Gobartt E, Escalona R, Usieto S, Marti E, 2017 Shh-mediated centrosomal recruitment of PKA promotes symmetric proliferative neuroepithelial cell division. Nat Cell Biol 19, 493–503. [PubMed: 28446817]

Saade M, Gutierrez-Vallejo I, Le Dreau G, Rabadan MA, Miguez DG, Buceta J, Marti E, 2013 Sonic hedgehog signaling switches the mode of division in the developing nervous system. Cell Rep 4, 492–503. [PubMed: 23891002]

Sahara S, O'Leary DD, 2009 Fgf10 regulates transition period of cortical stem cell differentiation to radial glia controlling generation of neurons and basal progenitors. Neuron 63, 48–62. [PubMed: 19607792]

Sarkisian MR, Bartley CM, Chi H, Nakamura F, Hashimoto-Torii K, Torii M, Flavell RA, Rakic P, 2006 MEKK4 signaling regulates filamin expression and neuronal migration. Neuron 52, 789–801. [PubMed: 17145501]

Shikata Y, Okada T, Hashimoto M, Ellis T, Matsumaru D, Shiroishi T, Ogawa M, Wainwright B, Motoyama J, 2011 Ptch1-mediated dosage-dependent action of Shh signaling regulates neural progenitor development at late gestational stages. Dev Biol 349, 147–159. [PubMed: 20969845]

Shimada IS, Acar M, Burgess RJ, Zhao Z, Morrison SJ, 2017 Prdm16 is required for the maintenance of neural stem cells in the postnatal forebrain and their differentiation into ependymal cells. Genes & development 31, 1134–1146. [PubMed: 28698301]

Shimada IS, Hwang SH, Somatilaka BN, Wang X, Skowron P, Kim J, Kim M, Shelton JM, Rajaram V, Xuan Z, Taylor MD, Mukhopadhyay S, 2018 Basal Suppression of the Sonic Hedgehog Pathway by the G-Protein-Coupled Receptor Gpr161 Restricts Medulloblastoma Pathogenesis. Cell Rep 22, 1169–1184. [PubMed: 29386106]

Shimamura K, Hartigan DJ, Martinez S, Puelles L, Rubenstein JL, 1995 Longitudinal organization of the anterior neural plate and neural tube. Development 121, 3923–3933. [PubMed: 8575293]

Spassky N, Han YG, Aguilar A, Strehl L, Besse L, Laclef C, Ros MR, Garcia-Verdugo JM, Alvarez-Buylla A, 2008 Primary cilia are required for cerebellar development and Shh-dependent expansion of progenitor pool. Dev Biol 317, 246–259. [PubMed: 18353302]

Spassky N, Merkle FT, Flames N, Tramontin AD, Garcia-Verdugo JM, Alvarez-Buylla A, 2005 Adult ependymal cells are postmitotic and are derived from radial glial cells during embryogenesis. J Neurosci 25, 10–18. [PubMed: 15634762]

Sun T, Hevner RF, 2014 Growth and folding of the mammalian cerebral cortex: from molecules to malformations. Nat Rev Neurosci 15, 217–232. [PubMed: 24646670]

Tronche F, Kellendonk C, Kretz O, Gass P, Anlag K, Orban PC, Bock R, Klein R, Schutz G, 1999 Disruption of the glucocorticoid receptor gene in the nervous system results in reduced anxiety. Nat Genet 23, 99–103. [PubMed: 10471508]

Tuson M, He M, Anderson KV, 2011 Protein kinase A acts at the basal body of the primary cilium to prevent Gli2 activation and ventralization of the mouse neural tube. Development 138, 4921–4930. [PubMed: 22007132]

Wang H, Ge G, Uchida Y, Luu B, Ahn S, 2011 Gli3 is required for maintenance and fate specification of cortical progenitors. The Journal of neuroscience : the official journal of the Society for Neuroscience 31, 6440–6448.

Wang H, Kane AW, Lee C, Ahn S, 2014 Gli3 repressor controls cell fates and cell adhesion for proper establishment of neurogenic niche. Cell Rep 8, 1093–1104. [PubMed: 25127137]

Wang L, Hou S, Han YG, 2016 Hedgehog signaling promotes basal progenitor expansion and the growth and folding of the neocortex. Nat Neurosci 19, 888–896. [PubMed: 27214567]

Weller RO, Kida S, Zhang ET, 1992 Pathways of fluid drainage from the brain--morphological aspects and immunological significance in rat and man. Brain Pathol 2, 277–284. [PubMed: 1341963]

Wen X, Lai CK, Evangelista M, Hongo JA, de Sauvage FJ, Scales SJ, 2010 Kinetics of hedgehog-dependent full-length Gli3 accumulation in primary cilia and subsequent degradation. Mol Cell Biol 30, 1910–1922. [PubMed: 20154143]

Willaredt MA, Hasenpusch-Theil K, Gardner HA, Kitanovic I, Hirschfeld-Warneken VC, Gojak CP, Gorgas K, Bradford CL, Spatz J, Wolfl S, Theil T, Tucker KL, 2008 A crucial role for primary cilia in cortical morphogenesis. J Neurosci 28, 12887–12900. [PubMed: 19036983]

Wilson SL, Wilson JP, Wang C, Wang B, McConnell SK, 2012 Primary cilia and Gli3 activity regulate cerebral cortical size. Dev Neurobiol 72, 1196–1212. [PubMed: 21976438]

Wolpert L, 1969 Positional information and the spatial pattern of cellular differentiation. J Theor Biol 25, 1–47. [PubMed: 4390734]

Yabut OR, Fernandez G, Huynh T, Yoon K, Pleasure SJ, 2015 Suppressor of Fused Is Critical for Maintenance of Neuronal Progenitor Identity during Corticogenesis. Cell Rep 12, 2021–2034. [PubMed: 26387942]

Yabut OR, Ng HX, Fernandez G, Yoon K, Kuhn J, Pleasure SJ, 2016 Loss of Suppressor of Fused in Mid-Corticogenesis Leads to the Expansion of Intermediate Progenitors. J Dev Biol 4.

Yu W, Wang Y, McDonnell K, Stephen D, Bai CB, 2009 Patterning of ventral telencephalon requires positive function of Gli transcription factors. Dev Biol 334, 264–275. [PubMed: 19632216]

Zhuo L, Theis M, Alvarez-Maya I, Brenner M, Willecke K, Messing A, 2001 hGFAP-cre transgenic mice for manipulation of glial and neuronal function in vivo. Genesis 31, 85–94. [PubMed: 11668683]

Highlights

- Deleting *Gpr161* in mid-gestation causes derepression of Shh signaling in forebrain.
- Hydrocephalus was apparent by birth without defects in ependymal cells or aqueduct.
- Hydrocephalus was caused by ventriculomegaly from radial glial overproliferation.
- Polymicrogyria, increased intermediate progenitors and basal radial glia were seen.
- Periventricular nodular heterotopia resulted from neuronal migration defects.

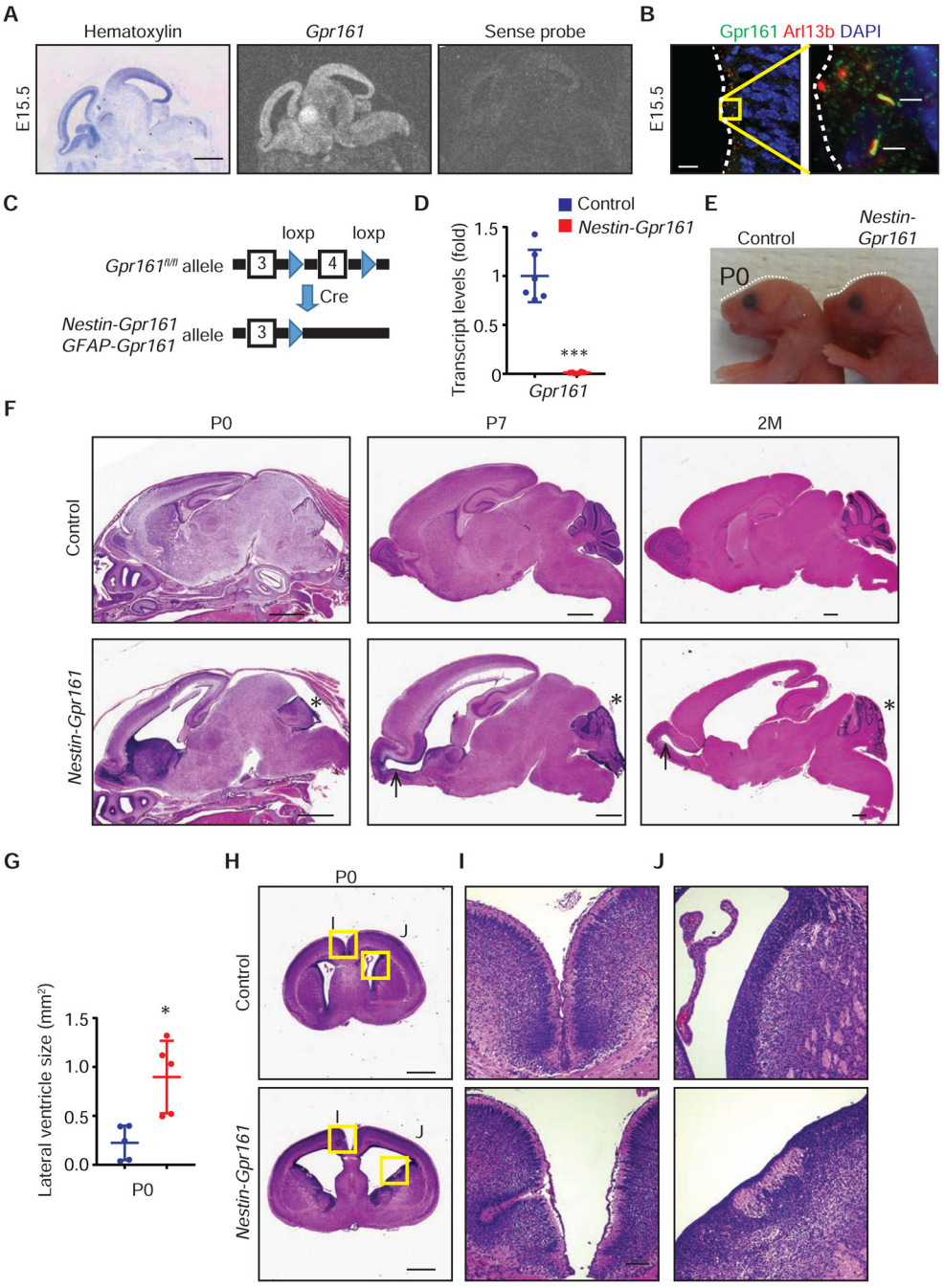

Figure 1. Lack of *Gpr161* in forebrain during mid-gestation causes hydrocephalus, periventricular heterotopia and polymicrogyria.

(**A**) Broad expression of *Gpr161* in the E15.5 embryonic brain by radioisotopic *in situ* hybridization using anti-sense probe. Hematoxylin staining shows the sagittal brain morphology. Sense probe is a negative control.

(**B**) Gpr161 localizes to the primary cilia of radial glia in the medial wall of the ventricular zone at E15.5. Arrows point to cilia.

(**C**) Schematic showing *Gpr161* exon 4 deletion with *Nestin-Cre* allele (*Nestin-Gpr161* cko) or *hGFAP-Cre* allele (*GFAP-Gpr161*).

(**D**) *Gpr161* transcript levels in the cortex by qRT-PCR at E14.5 (n=6 mice each).
(**E**) Representative picture showing control mouse heads and domed heads of *Nestin-Gpr161* cko mice at P0.
(**F**) Hematoxylin and eosin-stained sagittal sections showing enlarged lateral ventricles at P0, P7 and 2 month old adult brains of *Nestin-Gpr161* cko mice. Asterisks point to cerebellar hyperproliferation and dysplasia. Arrows depict the expansion of lateral ventricular wall extending into the subependymal layer in the olfactory bulb.
(**G**) Increased lateral ventricle area in *Nestin-Cre; Gpr161*$^{fl/fl}$ mice as compared to the littermate control mice at P0 (n=5 mice each, only one side counted/mice).
(**H**-**J**) Hematoxylin and eosin-stained coronal sections showing enlarged ventricles, (**I**) gyrus in the cingulate cortex (white arrow) and (**J**) periventricular heterotopia (white arrow) at P0 of the brain of *Nestin-Gpr161* cko mice.
All data represent mean ± SD. Scale bars are (**A**, **F**, **H**) 1 mm and (**B**) 10 μm and (**I** and **J**) 100 μm. Nuclei are stained by DAPI. *, $p<0.05$ and ***, $p<0.001$ by student's *t*-test. Also see Figure S1 and supplementary movies 1–4.

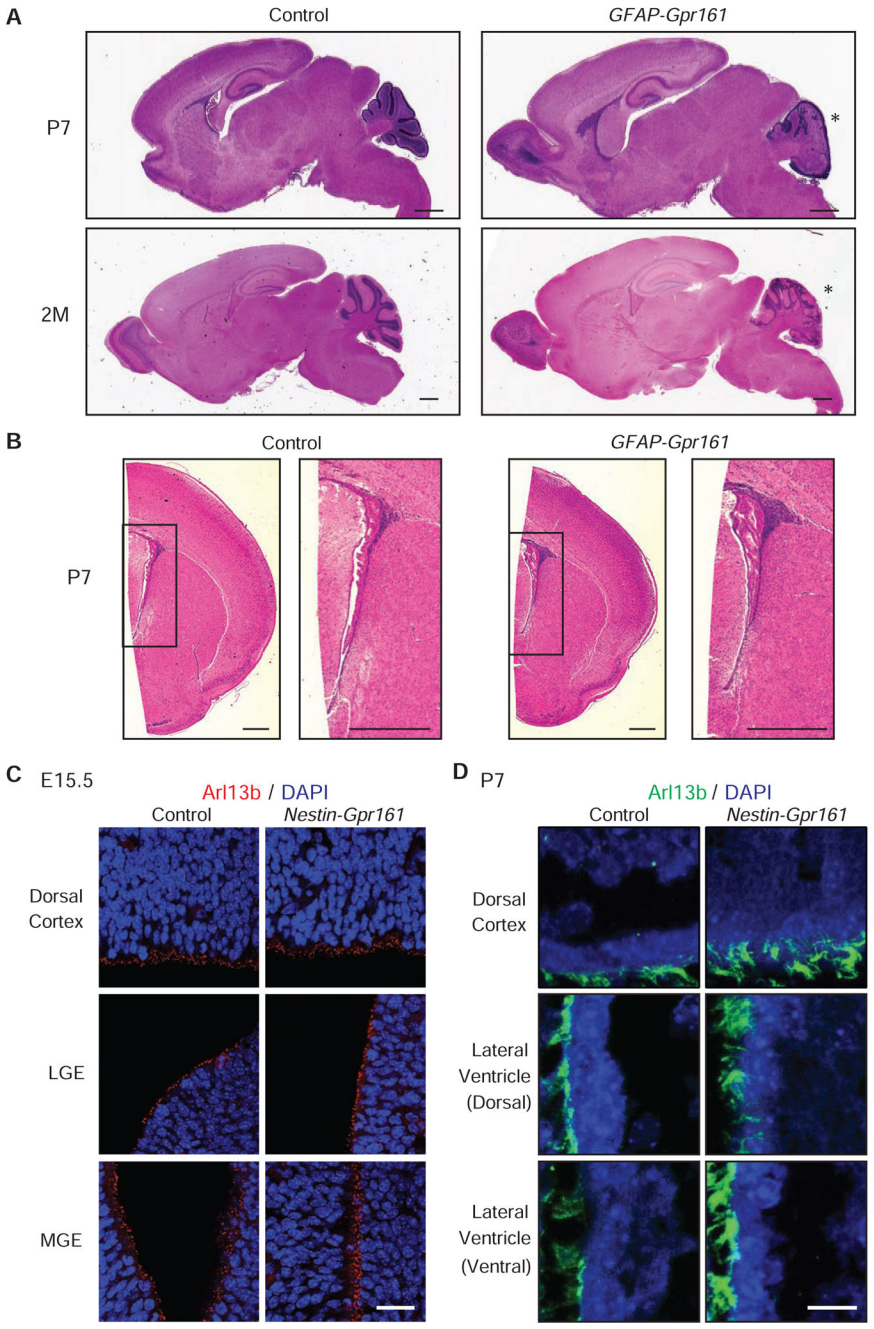

Figure 2. Late midgestational deletion of *Gpr161* in neuroprogenitors does not grossly affect the forebrain.

(**A**) Hematoxylin and eosin-stained sagittal sections showing normal brain morphology at P7 and adult brains of *hGFAP-Cre; Gpr161*$^{fl/fl}$ (*GFAP-Gpr161* cko) mice. Asterisks point to cerebellar hyperproliferation and dysplasia. Scale, 1 mm.

(**B**) Hematoxylin and eosin-stained coronal sections showing normal brain morphology with no periventricular heterotopia or hydrocephalus at P7 of the brain of *GFAP-Gpr161* cko mice. Scale, 500 μm.

(**C**) Normal cilia in control (*Gpr161*$^{f/+}$) and *Nestin-Gpr161* cko in the cortical surface and lateral/medial ganglionic eminences (LGE/MGE) at P0 shown by immunostaining of Arl13b. Scale, 10 μm.

(**D**) Normal ependymal cell motile cilia in control (*Gpr161*$^{f/f}$) and *GFAP-Gpr161* cko in the cortical surface and dorsal or ventral regions of lateral ventricles at P7 shown by immunostaining of Arl13b. Scale, 10 μm.

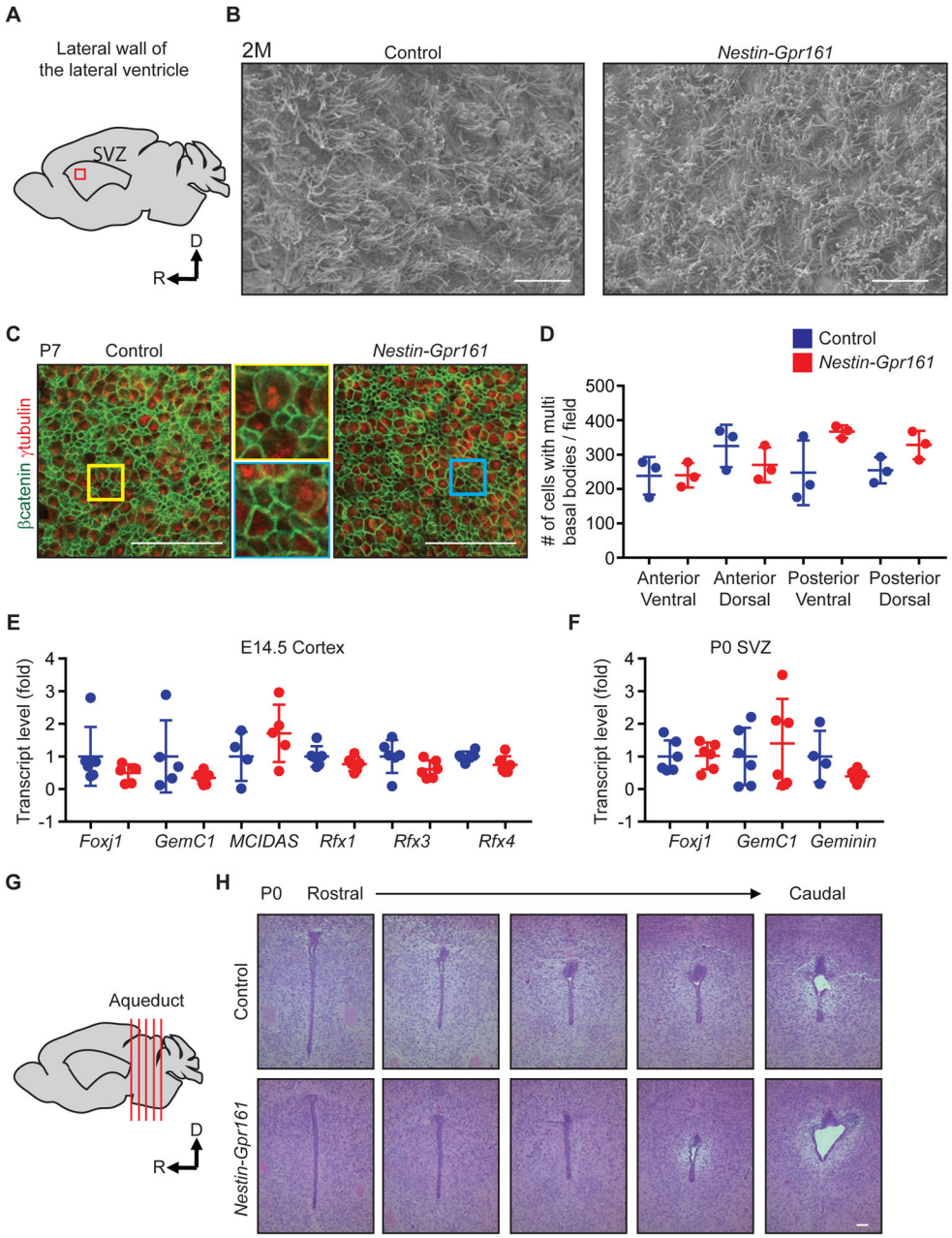

Figure 3. *Gpr161* deletion causes hydrocephalus despite lack of ependymal cell or aqueductal defects.

(A) Schematic showing sagittal section of mouse brain. The anterior dorsal region in the subventricular zone (SVZ) (red box) is analyzed in **B** and **C**. Images from other regions in Figure S2.

(**B**) Scanning electron microscope revealed abundant ciliated ependymal cells in mice (2 months old) of both genotypes.

(**C**) γtubulin^{+} multiple basal bodies were observed in the SVZ in the larger size ependymal cells at P7 in *en face* view (white arrows). β-catenin marks the cell boundaries. Smaller apical processes contain single centrosomes and are from radial glia.

(**D**) The number of cells which contain multiple basal bodies in the SVZ was quantified at P7 (n=3 mice each).
(**E**, **F**) qRT-PCR analysis of transcription factors that are critical for ependymal cell differentiation in the cortex at E14.5 and SVZ at P0. n=4–6 mice each.
(**G**) Schematic showing sagittal section of P0 mouse brain. The red lines are the coronal sections analyzed in **H**.
(**H**) Serial coronal sections of the aqueduct show no differences between genotypes.
All data represent mean ± SD. D indicates dorsal and R indicates rostral. Scale bars are (**B**) 10 μm and (**C and H**) 100 μm. Also see Figure S1.

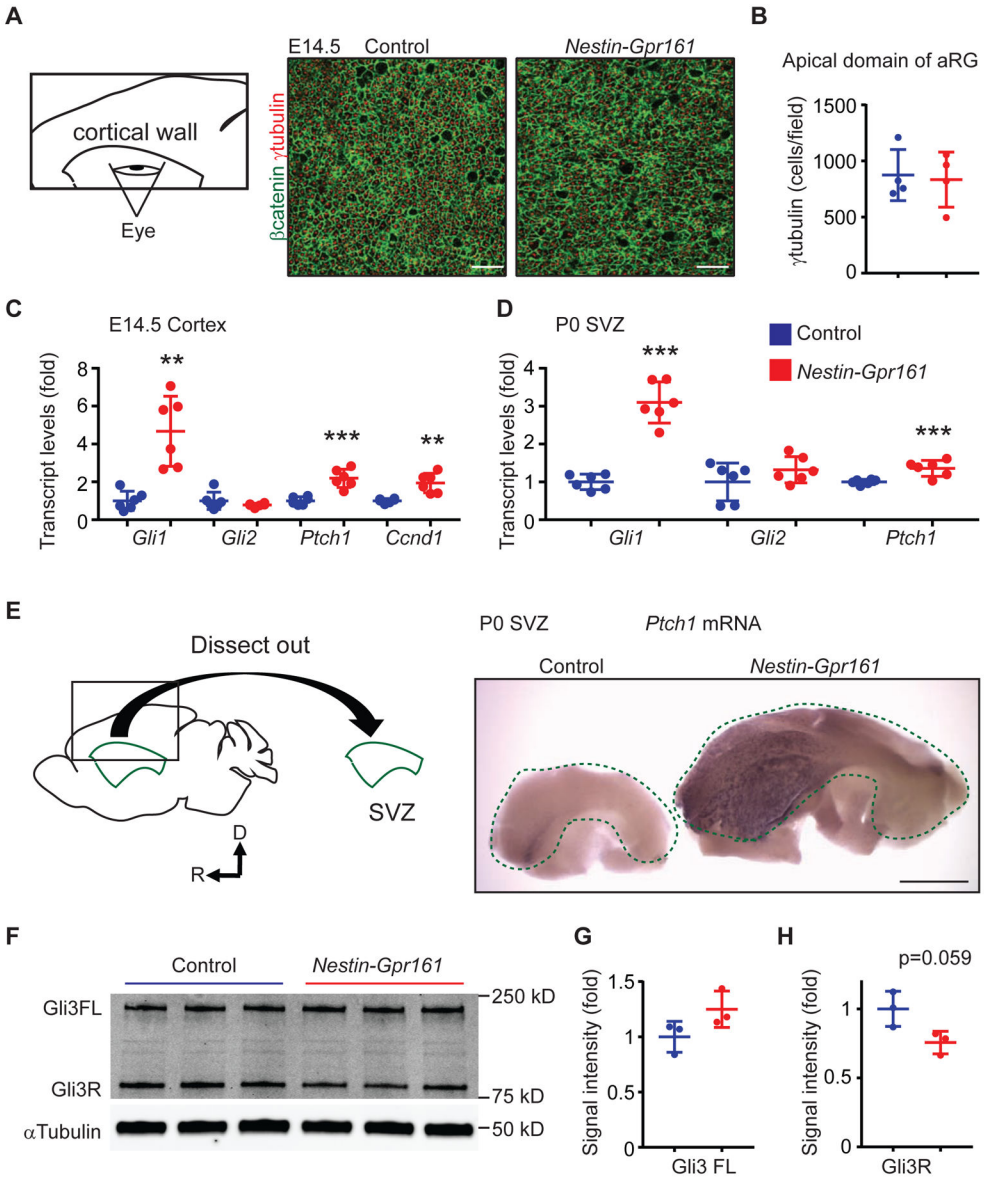

Figure 4. Increased Shh pathway activity in *Gpr161* cko telencephalon.

(**A**, **B**) Apical process of apical radial glia (aRG) are shown by γtubulin (centrosome) and β catenin (intercellular contacts) immunostaining on the ventricular surface of the cortex at E14.5 in *en face* view. Quantification of apical processes with n=3 mice each.

(**C**, **D**) qRT-PCR analysis of Shh target transcript levels in the cortex at E14.5 and SVZ at P0. n=6 each.

(**E**) Increased expression of *Ptch1* transcript levels in the P0 SVZ by RNA *in situ* hybridization. Note that *Ptch1* transcripts are expressed only in the anterior ventral area of control SVZ, but broadly expressed in *Nestin-Gpr161* cko SVZ, which is also larger in size.

(**F-H**) Immunoblotting for Gli3 and quantification (after normalization with atubulin levels) in E15.5 cortex of *Nestin-Gpr161* cko and littermate controls (n=3 each).

Scale bars are (**A**) 10 μm and (**E**) 1 mm. **, p<0.01 and ***, p<0.001 by student's *t*-test.

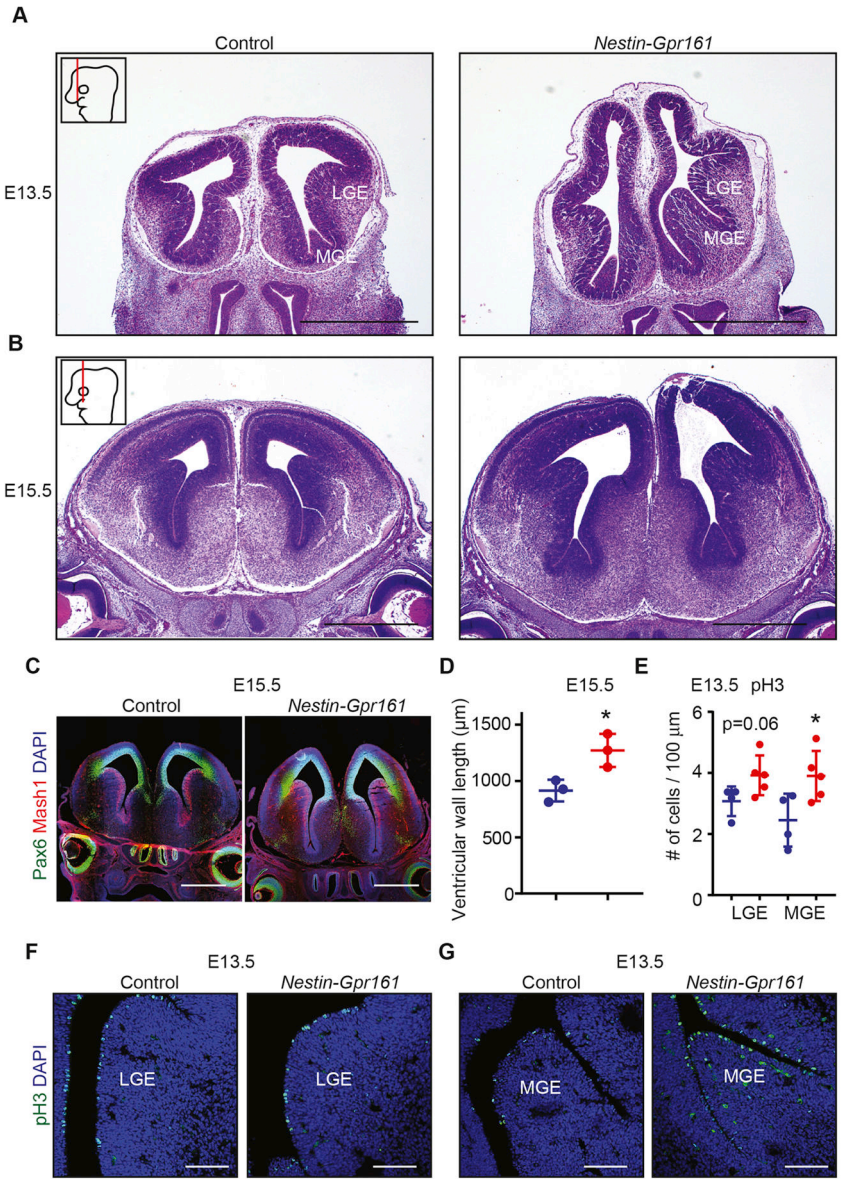

Figure 5. *Gpr161* deletion induced ventriculomegaly by late mid-gestation.

(**A**, **B**) Hematoxylin and eosin-stained coronal sections showing enlarged lateral ventricles of E13.5 and E15.5 brains of *Nestin-Gpr161* cko mice.

(**C**) Dorsoventral patterning of coronal sections as in (B) by dorsal marker (Pax6) and ventral marker (Mash1) is not grossly affected at E15.5.

(**D**) The ventricular wall length of the lateral ventricle at E15.5 was increased in *Nestin-Gpr161* cko. 5–6 DAPI stained sections (150 m apart) starting from just anterior to the eye were used for the ventricular wall length quantification. N=3 mice each, only one side/mice counted.

(**E-G**) The number of mitotic cells increased in the ganglionic eminences of the lateral ventricle of *Nestin-Gpr161* cko at E13.5. L/MGE, lateral/medial ganglionic eminence. Scale bars are (**A**, **B**, **C**) 1 mm and (**F**, **G**) 100 μm. *, p<0.05 by student's *t*-test. Also see Figure S2 and supplementary movies 5–7.

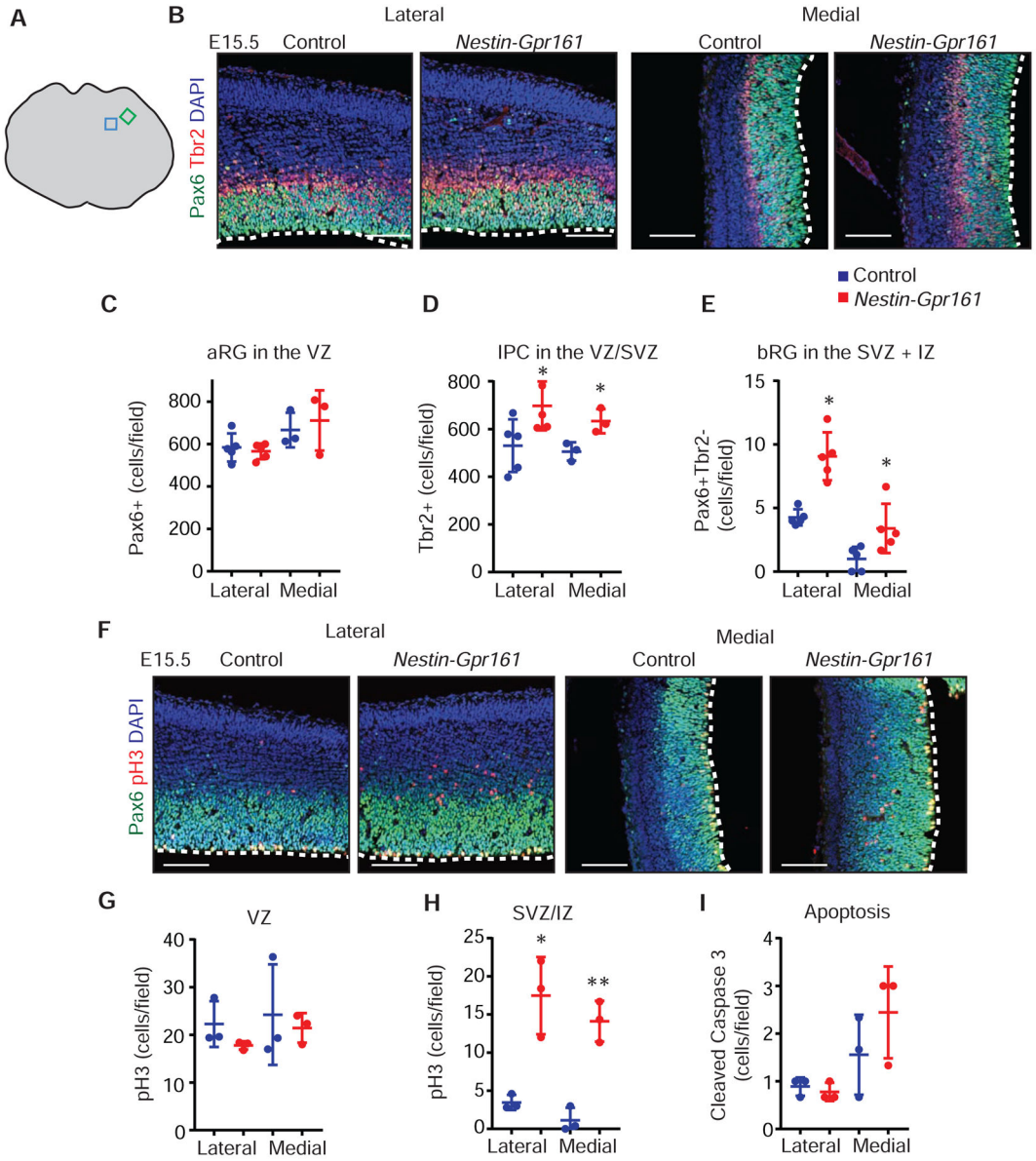

Figure 6. *Gpr161* deletion expands intermediate progenitor cells and basal radial glia at the expense of radial glia.

(**A**) Schematics of coronal section of mouse brain at E15.5. The green and blue square boxes denote lateral and medial regions shown in (**B**) and (**F**), respectively.

(**B**) Pax6-positive radial glia and Tbr2-positive intermediate progenitor cells (IPCs) in E15.5 cortex in lateral and medial regions.

(**C**) Pax6 positive apical radial glia (aRG) in the VZ/SVZ were similar between *Nestin-Gpr161* cko mice and littermate control at E15.5. N=5 each (lateral) and 3 each (medial).

(**D**) The number of Tbr2-positive IPCs were increased in *Nestin-Gpr161* cko mice as compared to littermate control at E15.5. N=5 each (lateral) and 3 each (medial).

(**E**) Pax6-positive Tbr2-negative basal radial glia (bRG) were increased in *Nestin-Gpr161* cko mice as compared to littermate control at E15.5. N=5 mice each.

(**F**) Pax6-positive aRG and pH3 positive mitotic cells in E15.5 cortex in lateral and medial regions.

(**G**) The numbers of pH3-positive cells in the VZ were similar between genotypes. n=3 mice each.

(**H**) The numbers of pH3-positive mitotic cells were increased in the SVZ/IZ at E15.5. n=3 mice each.

(**I**) The number of apoptotic cells was similar between backgrounds at E15.5. n=3 mice each.

All data represent mean ± SD. Nuclei are stained by DAPI. Scale bars are (**B** and **F**) 100 μm. *, $p<0.05$ and **, $p<0.01$ by student's *t*-test. Abbreviations: CP, cortical plate; IZ, intermediate zone; SVZ, subventricular zone; VZ, ventricular zone.

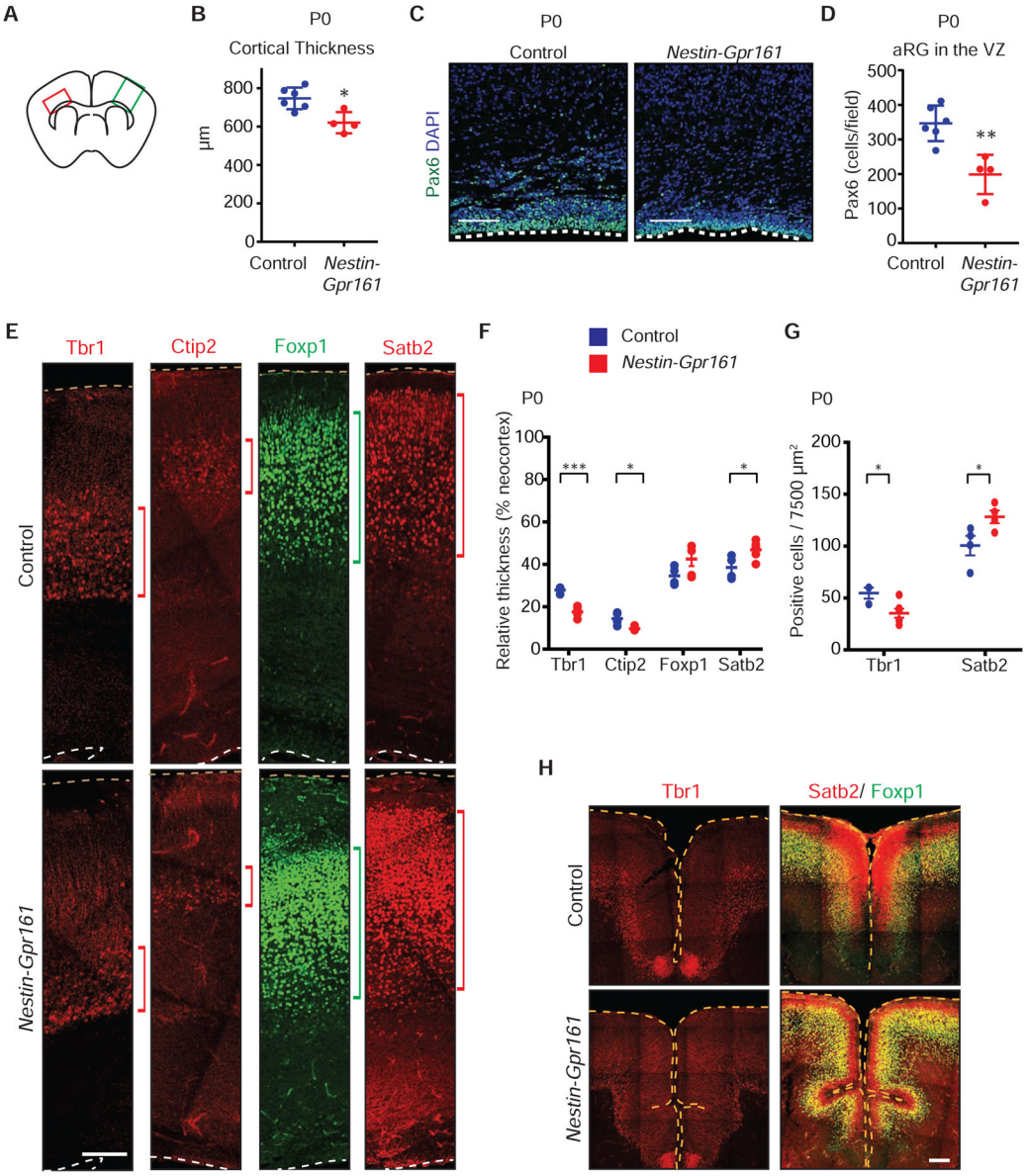

Figure 7. *Gpr161* deletion regulates cortical lamination.

(**A**) Schematic showing the regions analyzed at P0 (red box, **C-D**; green box, **B**, **E-G**).

(**B**) The lateral cortical thickness was measured in three to five coronal sections per mouse at P0. The thickness was measured from the dorso-lateral part of the lateral ventricle to the cortical surface. n=4–6 mice each.

(**C, D**) The number of Pax6-positive aRG in the VZ/SVZ in P0 lateral cortex. n=4–6 mice each.

(**E**) Relative thickness of Tbr1 (layer VI), Ctip2 (layer V), Satb2 (layers II-III) abd FoxP1 (layers III-V) positive cells are shown with respect to thickness of the neocortex at P0. Brown and white broken lines show pial and ventricular surface, respectively.

(**F**) Quantification of relative thickness of Tbr1, Ctip2 and Satb2 positive cells in (**E**) are shown with respect to thickness of the neocortex at P0. n=3–6 hemispheres from 2 control

(*Gpr161*$^{f/f}$) or 3 *Nestin-Gpr161* cko mice. Each dot represents data from a separate hemisphere.

(**G**) Quantification of absolute number of Tbr1 (in layer VI) and Satb2 positive cells (in layer II) in a 7500 μm^2 surface area of sections shown in (**E**). n=3–6 hemispheres from 2 control (*Gpr161*$^{f/f}$) or 3 *Nestin-Gpr161* cko mice. Each dot represents data from a separate hemisphere.

(**H**) The cingulate cortex showed folding of cortex with Satb2 and FoxP1 positive neurons in the polymicrogyric region.

Tiled images in (**E**) and (**H**). All data represent mean ± SD (**B**, **D**) or SEM (**F**, **G**). Nuclei are stained by DAPI. Scale bar **C**, **E, H** 100 μm. *, p<0.05; **, p<0.01; ***, p<0.001 by student's *t*-test. Abbreviations: IZ, intermediate zone; SVZ, subventricular zone; VZ, ventricular zone.

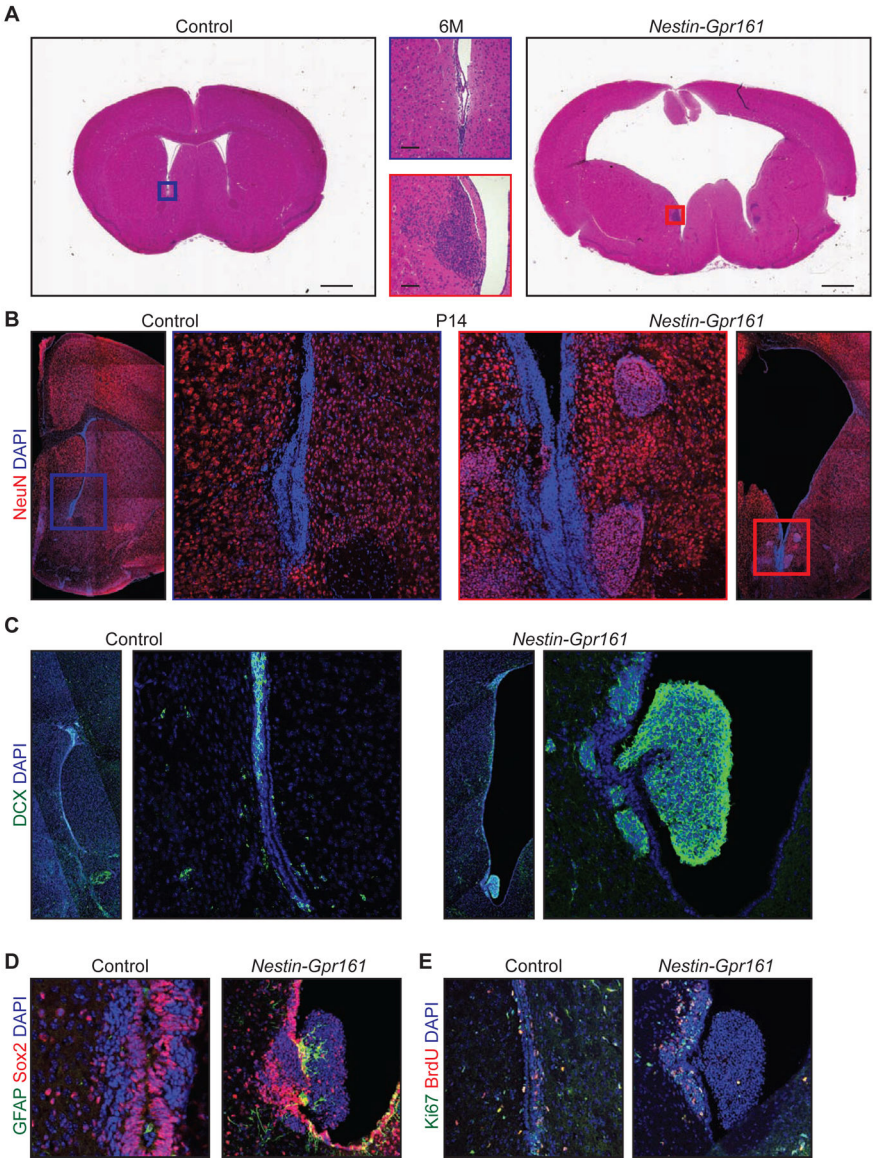

Figure 8. *Gpr161* deletion induced periventricular nodular heterotopia.

(**A**) Hematoxylin and eosin-stained coronal sections of lateral ventricles showing periventricular heterotopia in the brains of *Nestin-Gpr161* cko mice at 6 months old. Blue and red boxes are enlarged in the center.

(**B**) Periventricular heterotopia is stained with NeuN in the brains of *Nestin-Gpr161* cko mice at P14. Blue and Red boxes are enlarged in the center.

(**C-E**) Periventricular heterotopic nodule (insets of lateral ventricular region, left, shown in right panels in C) is positive for doublecortin (DCX) (C), negative for astrocyte marker GFAP (D), sparsely positive for Sox2 (D) or negative for proliferation markers (E) in *Nestin-Gpr161* cko mice at P14.

Scale bars are (**A**) 1 mm and (**B-E**) 100 μm.

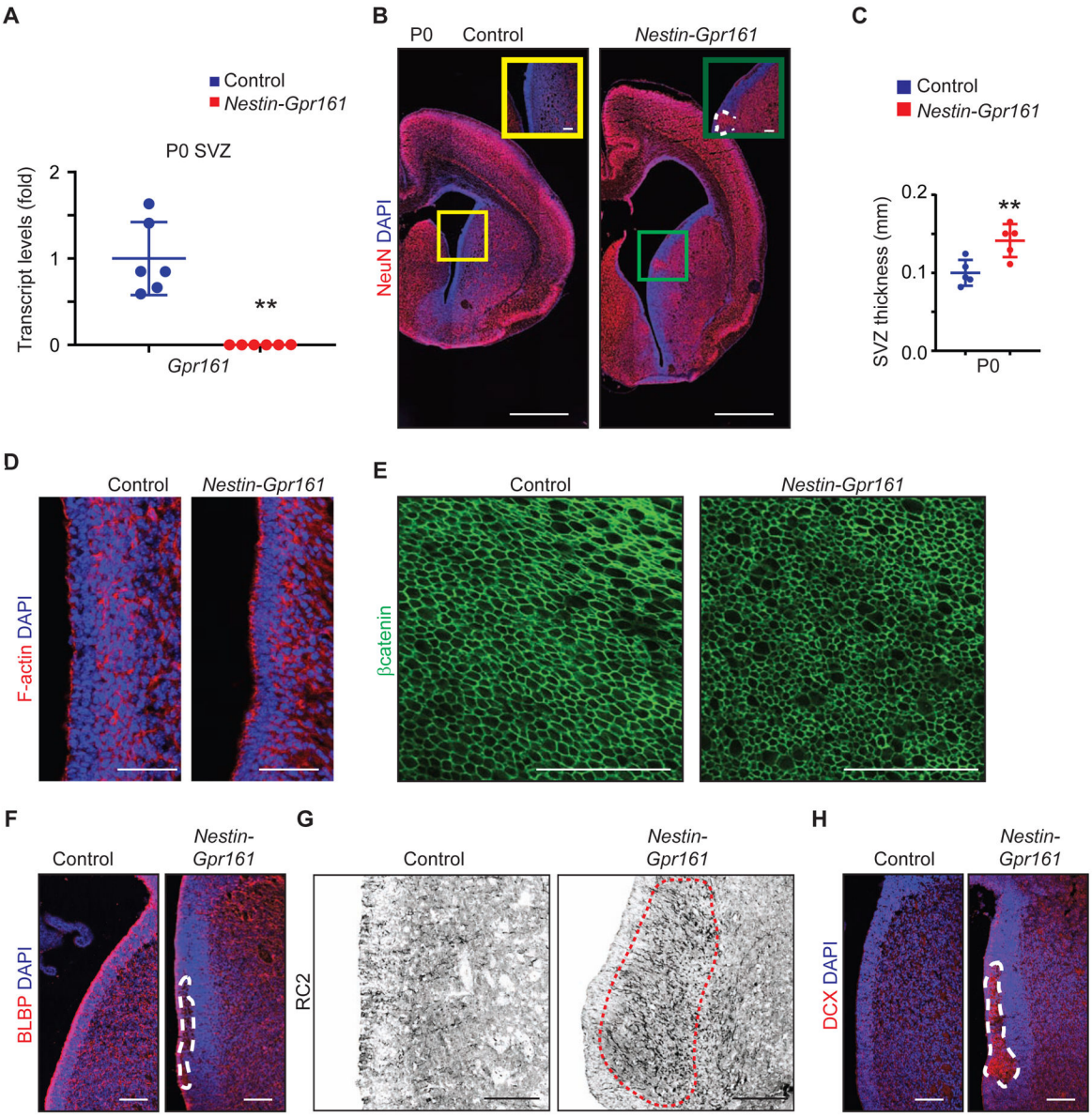

Figure 9. Periventricular nodular heterotopia arising from neuron-intrinsic migration defects upon *Gpr161* deletion.

(A) *Gpr161* transcript levels in the SVZ by qRT-PCR at P0 (n=6 each).

(B) Periventricular heterotopia is stained with NeuN in the brains of *Nestin-Gpr161* cko mice at P0. Yellow and green boxes are enlarged in insets. Heterotopic area marked by white broken line.

(**C**) Increased SVZ thickness in *Nestin-Gpr161* cko compared to littermate control mice at P0 (n=5 each). The thickness was measured at the dorsal part of the lateral ventricle.

(D) Apical anchoring of cells lining the ventricles was not disrupted at P0 as examined by Phalloidin staining.

(E) βcatenin marked intact cell boundaries of apical processes of radial glia in lateral ventricles (*en face* view).

(F) The radial glial fibers seen by BLBP immunostaining were unperturbed in *Nestin-Gpr161* cko at P0. Heterotopic area marked by white broken line.
(G) Radial glial fibers seen by immunostaining using anti-radial glial cell marker-2 antibody, clone RC2 were unperturbed even in heterotopic areas (marked by red broken line) in *Nestin-Gpr161* cko at P0. Inverted grey scale image for RC2 is shown.
(H) Accumulation of doublecortin-positive differentiating neurons (marked by white broken line) was observed in the SVZ of *Nestin-Gpr161* cko mice at P0.
Data represent mean ± SD. **, $p<0.01$ by student's *t*-test. Scale bars are (**B**) 1 mm and 100 μm in insets, (**D-H**) 100 μm.

A

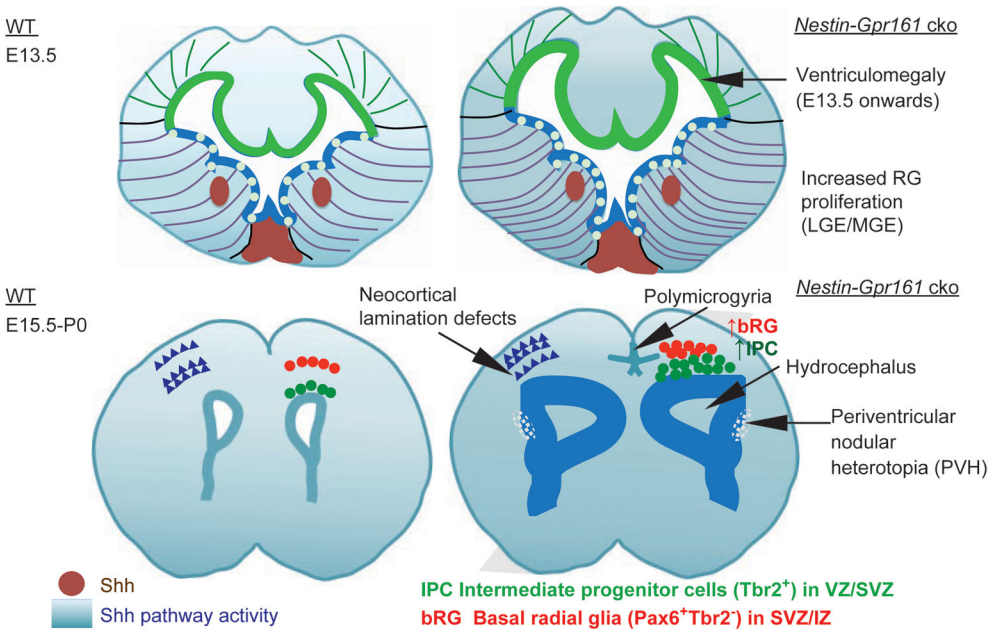

B

	Inactivation in cortex by	Ventriculomegaly /Hydrocephalus	IPC production	bRG production	Cortical lamination	Polymicrogyria	PVH	Reference
***Nestin-Gpr161* cko**	E10.5	Present	↑	Increased	↑ Upper, ↓ deep layers	Cingulate cortex	Present	This paper
***GFAP-Gpr161* cko**	E13.5	Absent	?	?	?	?	Absent	This paper
***Emx1-SmoM2* cko**	E10.5	?	↓	?	Disorganized, ↓upper layers	?	?	*Yabut et al., 2015*
***GFAP-SmoM2* cko**	E13.5	Absent	↑	Increased	↑ Upper, ↓ deep layers (Cingulate, medial cortex only)	Cingulate cortex	Absent	*Wang et al., 2016; Yabut et al., 2015*
***Nestin-SmoM2* cko**	E10.5	Absent	?	?	?	Cingulate and lateral cortex	Absent	*Wang et al., 2016*
***Nestin-Ptch1* cko**	E10.5	Extensively folded & distorted	?	?	No cortical plate (Die at E15.5)	?	?	*Dave et al., 2011*
***Emx1-Sufu* cko**	E10.5	Present	↓	?	Disorganized, ↓upper layers	?	?	*Yabut et al., 2015*
***GFAP-Sufu* cko**	E13.5	Absent	↑	?	Almost unaffected	?	?	*Yabut et al., 2016*
***Emx1-Gli3* cko**	E10.5	?	↓ (E11.5) ↑(E12.5)	?	Slight ↑ upper, ↓ deep layers	?	?	*Hasenpusch-Theil et al., 2018*
***Nestin-Gli3* cko**	E10.5	Absent	↓ (E18.5)	?	↓ Upper, ↑ deep layers	?	?	*Wang et al., 2011, 2014*

Figure 10. Effects of derepression of Shh signaling in forebrain.

(A) Cartoon summarizing phenotypes and mechanisms underlying the phenotypes in *Nestin-Gpr161* cko versus wild type (WT). Abbreviations: LGE, lateral ganglionic eminence; MGE, medial ganglionic eminence; RG, radial glia; IZ, intermediate zone; SVZ, subventricular zone; VZ, ventricular zone.

(B) Table comparing different phenotypes between strains that cause increased Shh signaling in forebrain. *Nestin-Gpr161* cko-specific phenotypes such as ventriculomegaly, periventricular heterotopia, and polymicrogyria likely arise from high Shh signaling in radial glia during early mid-gestation. ?, unknown.